HOT DYNAMIC CONSOLIDATION OF AlFeVSi ALLOY POWDERS

A THESIS SUBMITTED TO
THE GRADUATE SCHOOL OF NATURAL AND APPLIED SCIENCES
OF
MIDDLE EAST TECHNICAL UNIVERSITY

BY

ŞEVKİYE EZGİ KOTAN

IN PARTIAL FULFILLMENT OF THE REQUIREMENTS
FOR
THE DEGREE OF MASTER OF SCIENCE
IN
METALLURGICAL AND MATERIALS ENGINEERING

APRIL 2005

Approval of the Graduate School of Natural and Applied Sciences

_____

Prof. Dr. Canan ÖZGEN

Director

I certify that this thesis satisfies all the requirements as a thesis for the degree of Master of Science.

_____

Prof. Dr. Tayfur ÖZTÜRK

Head of Department

This is to certify that we have read this thesis and that in our opinion it is fully adequate, in scope and quality, as a thesis for the degree of Master of Science.

_____   _____

Prof. Dr. Filiz SARIOĞLU   Prof. Dr. Ali KALKANLI

Co-Supervisor   Supervisor

Examining Committee Members

Prof. Dr. Haluk ATALA   (METU, METE)   _____

Prof. Dr. Ali KALKANLI   (METU, METE)   _____

Prof. Dr. Filiz SARIOĞLU   (METU, METE)   _____

Prof. Dr. Şakir BOR   (METU, METE)   _____

Assoc. Prof. Dr. Tamer ÖZDEMİR   (GAZİ UNV)   _____

I hereby declare that all information in this document has been obtained and presented in accordance with academic rules and ethical conduct. I also declare that, as required by these rules and conduct, I have fully cited and referenced all material and results that are not original to this work.

Name, Last name : Şevkiye Ezgi Kotan

Signature :

ABSTRACT

HOT DYNAMIC CONSOLIDATION OF AlFeVSi ALLOY POWDERS

Kotan, Şevkiye Ezgi

M.Sc. Department of Metallurgical and Materials Engineering

Supervisor: Prof. Dr. Ali Kalkanlı

Co-Supervisor: Prof. Dr. Filiz Sarıoğlu

April 2005, 94

The experimental alloy powders of 1% Mg treated Al-8Fe-1.8V-8Si were obtained by air atomization. The screen analysis of powders was made by sieves with meshes ranging from +90μm, +63μm, +53μm, +45μm, +38μm to -38μm.

Unreinforced and TiC particulate reinforced specimens were produced by hot dynamic consolidation which is known as hot swaging. Powders were canned into pure aluminium tubes of about 10cm length and 2.2cm diameter. Single action and double action cold pressing were applied to some of the specimens before hot dynamic compaction and some specimens of canned loose powder were also processed. The diameters of the hot compacts were decreased in a two step process by swaging machine (rotary dynamic compaction). During the first step, after canning, compacts had been held at 480°C for 1 hour and swaged, thus the diameter decreased from 2.2 cm to 1.97cm. Secondly, the compacts were reheated to 480ºC and held for 1 hour and further swaged to obtain a diameter decrease from 1.97cm to 1.54cm.

Generally, the microstructures of the hot dynamic compacted specimens were homogeneous except the specimens produced by using -63 μm +53 μm powder size fraction. By SEM study, a vanadium free cross like AlFeSi phase was observed near the outer regions of the specimen. No considerable coarsening of the dispersoids was observed after hot dynamic compaction of +63 μm size powder. For -90μm +63μm size powders, maximum flexural strength values obtained by three point bending test increased by addition of 10% TiC to from 152 MPa to 285 MPa at double pressed condition and from 76MPa to 190MPa at loose powder canning condition. By hardness tests, it was observed that hardness values were inversely proportional to powder size and increased from 107 BHN to 147 BHN for corresponding powder size range of +90μm to -38μm. Porosity values obtained by Archimedes principle for single pressing varied between 0.03 % and 1.10% for corresponding size range of +38μm to +90μm. No considerable porosity was detected for double pressing. Porosity values of canned loose powder were between 3% and 10% for the range of +38 μm- +45 μm. By X-Ray analysis, it was revealed that Mg_2Si reaction did not form after artificial aging of specimens up to 8 hours at 190°C. Also, x-ray analysis of individual powders and specimens obtained by hot dynamic compaction of the same powder showed that; after hot dynamic compaction, the alloy powders were stable and no new phase formation was detected for +63μm size. DSC examination of the specimens produced from +90μm, +63μm, +53μm, -38μm powder confirmed the microstructure stability up to the melting temperature. Melting temperature was detected to be in the range of 560°C-575°C by DSC .

Key words: High temperature stable AlFeVSi alloys, hot dynamic compaction, PM processing of aluminum alloys, TiC reinforced aluminum alloys

ÖZ

AlFeVSi ALAŞIM TOZUNUN SICAK DİNAMİK YOĞUNLAŞTIRILMASI

Kotan, Şevkiye Ezgi

M.Sc. Department of Metallurgical and Materials Engineering

Supervisor: Prof. Dr. Ali Kalkanlı

Co-Supervisor: Prof. Dr. Filiz Sarıoğlu

April 2005, 94

Test alaşımı olan %1 Mg eklenmiş Al-8Fe-1.8V-8Si alaşım tozu hava atomizasyonu ile elde edildi. Toz +90μm, +63μm, +53μm, +45μm, +38μm ve -38μm ölçülerinde elendi.

Sadece alaşım tozundan üretilen numuneler ile TiC ilavesi yapılan numuneler sıcak dinamik yoğunlaştırma yöntemi ile üretildi. Tozlar 10cm boyunda ve 2.2 cm çapında alüminyum tüplere dolduruldu. Sıcak yoğunlaştırmadan önce numunelerin bir kısmına tek yönlü, bir kısmına çift yönlü soğuk sıkıştırma uygulanırken, soğuk sıkıştırma yapılmayan numuneler de hazırlandı. Sıcak yoğunlaştırma sıcak dinamik dövücü ile yapıldı. Numunelerin çapı iki aşamada düşürüldü. Numuneler 480 ºC de 1 saat tutulduktan sonra çap önce 2.2 cm den 1.97cm ye, daha sonra yine 480 ºC de 1 saat bekletildikten sonra 1.97cm den 1.54 cm ye düşürüldü.

Genel olarak, mikroyapı -63 μm +53 μm boyutundaki tozdan üretilen numune dışında homojendi. Bu numunede dış kısımlarda çarpı şeklinde AlFeSi fazı gözlemlenmiştir. Sıcak dinamik yoğunlaştırmadan sonra çökelmiş faz çapında önemli bir değişiklik olmamıştır. Üç nokta bükme testi ile elde edilen kırılma

dayancı %10 TiC ilavesi ile çift yölü sıkıştırma yapılan numunelerde 152 MPa dan 285 MPa değerine, sıkıştırma yapılmayan numunelerde 76MPa dan 190MPa değerine yükselmiştir. Sertlik testleri ile toz boyutu ve sertliğin ters orantılı olduğu ve +90µm -38µm aralığında, sertlik değerlerinin 107BHN den 147 BHN ye yükseldiği gözlemlenmiştir. Arşimet yöntemiyle yapılan yoğunluk testleri ile tek yönlü sıkıştırılan numunelerde +38µm-+90µm aralığında yoğunlukta %0.03-1.10 oranlarında azalma olduğu, çift yönlü sıkıştırma yapılan numunelerde ise yoğunluk farkı bulunmadığı gözlemlenmiştir. Sıkıştırma yapılmayan numunelerin yoğunluğunda ise +38 µm ve +45 µm aralığında %3-10 oranlarında azalma olmuştur. X ışınları analizi ile 190°C de 8 saate kadar yapılan ısıl işlem sonucunda Mg_2Si oluşmadığı anlaşılmıştır. Ayrıca, +63µm boyutundaki toz ve bu tozdan üretilen numune için yapılan x ışınları analizi ile sıcak yoğunlaştırma sonrası yeni bir faz oluşmadığı görülmüştür. Termal analiz sonuçları +90µm, +63µm, +53µm ve -38µm boyutlarındaki tozdan üretilen numunelerde erime noktasına kadar mikroyapının kararlı olduğunu göstermiştir. Erime sıcaklıklarının 560°C-575°C aralığında olduğu yine termal analiz sonuçları ile belirlenmiştir.

Anahtar kelimeler: Yüksek sıcaklıkta kararlı AlFeVSi alaşımları, sıcak dinamik yoğunlaştırma, alümünyum alaşımlarında TM yöntemi, TiC takviyeli alüminyum alaşımları

To my family;

Mualla, Mustafa and Güher Kotan

ACKNOWLEDGEMENTS

TABLE OF CONTENTS

CHAPTER 1

INTRODUCTION

As a group of advanced materials, metal matrix composites have been developed for thirty years. [1] Physical and mechanical properties, and enhanced elevated temperature capabilities of metal matrix composites have made them attractive materials for aerospace, automotive and numerous other applications. [2, 3] However; non-uniform distribution of reinforcements and formability difficulties due to the limited room temperature ductility of composites hamper the use of some fabrication techniques. [3]

Because of the limitations of continuously reinforced materials, researches of discontinuously reinforced materials have been increasing. In fact, continuously reinforced materials offer better specific strength, but high strength fibers and their processing routes are extremely expensive and continuous fiber reinforced composites do not usually allow secondary forming process, which is used in the original shape in which they were manufactured. [4]

Discontinuously reinforced MMCs have some advantages as; availability of different reinforcements at competitive costs, successful manufacturing processes to produce reproducible structures and properties, existence of standard or near standard metal working methods to form MMCs [2].

Aluminum alloys are used as matrix for a long period of time both in research and in industrial applications. This is due to the lower cost of aluminum alloys when compared to the other low density alloys such as titanium and magnesium. [4] Al-Fe-Ce, Al-Cr-Zr, Al-Fe-Mo-V, Al-Fe-V-Si alloys obtained by rapid solidification and

age hardenable Al-Cu-Mg, Al-Zn-Mg-Cu and Al-Li alloys are some examples to this group of materials. [4, 5]

In aluminum matrix composites, commonly used reinforcements are ceramic particles like SiC and Al_2O_3 . Intermetallics have been used as reinforcements also in systems such as Ni-Al, Al-Fe. [4]

Different processes exist for the production of metal matrix composites. Powder metallurgy processes and high energy high rate processes are the solid state production methods. [2]. Powder metallurgy route has some advantages over ingot metallurgy such as;

 - The uniformity of reinforcement distribution improves the structural properties and reproducibility level in the properties.
- Strong interfacial reaction causing undesired reactions between matrix and the reinforcement is avoided by low processing temperature
- Materials that cannot be produced by any other alternative route can be produced by powder metallurgy technique, i.e. Ti alloys reinforced with SiC.
- Particle or whisker reinforced composites can be easily produced by P/M. [4]

P/M aluminum matrix composites present good mechanical properties when compared with those produced by other techniques [6].

CHAPTER 2

THEORY AND LITERATURE SURVEY

2.1. Particulate Reinforced MMC Composites

Among metal matrix composites, particulate reinforced MMCs have attracted considerable attention for aerospace, automobile and numerous other applications because of the relatively low costs, characteristics isotropic properties and development of various processing routes which result in reproducible microstructures and properties. [2]

Particle reinforced composites have two main differences from dispersion strengthened alloys; they have more volume fraction of reinforcement than the volume fraction of dispersoids in dispersion strengthened alloys and diameter of the particles and interparticle spacing are also in composite materials. [2, 7]

In particulate reinforced composites, matrix transfers the load to the particles and makes fabrication easier while reinforcing phase is the load bearing phase. Strength of particulate composites depends on the volume fraction of the reinforcement, the diameter of the particles and interparticle spacing. [7]

A general increase in strength is observed with the increase in volume fraction of the particles. Hard reinforcement produces high matrix constraint factors which are effective to prevent yielding in the matrix. [7]

Powder metallurgy is an advantageous way to fabricate particulate metal matrix composites because composites possess a higher dislocation density, a small subgrain size and limited segregation of particles especially compared to liquid state processes and as a result; superior mechanical properties obtained.[1,8]

2.2. Strengthening Behavior of Particulate Reinforced Composites

The addition of ceramic reinforcement particulates to metallic matrices generally leads to substantial increase in elastic modulus. Also, metal matrix composites exhibit combinations of tensile strength and abrasion resistance that are superior to those of the unreinforced matrices. [9]

Y. Wu et al. [9] stated that the overall increase in strength of MMC increases with decreasing matrix strength due to the fact that the matrix may deform extensively to accommodate large stress concentration without the nucleation of cracks. Experimental evidence of this phenomenon is presented in table 2.1.

Table2.1 Mechanical Properties of Aluminum Alloy Based MMC's [9]

Materials	Composition(wt%)				V_f(%)	Type of reinforcement	Processing	Temper	σ_{ys} (MPa)
Al-12Si					0	-	SDP	ST	101
Al-12Si/SiC					17.3	2p	SDP	ST	176
6061	Si	Cu	Mg	Cr	0	0	PM	T6	357
	0.6	0.28	1	0.2					
6061-SiC					20	3w	PM	T6	447
2014	Si	Cu		Mg	0	-	IM	T6	414
	0.8	4.4		0.5					
2014-SiC					20	p	PM	T6	481
8090	Li	Cu	Mg	Fe	0	-	IM	T6	480
	2.7	1.6	1.3	0.3					
	Zn	Si	Zr	Mn					
	0.25	0.2	0.16	0.1					
8090-SiC					12	p	PM	T6	486

SDP=spray deposition IM=Ingot Metallurgy PM=Powder Metallurgy

G. O'Donnal et al. [10] studied SiC particle reinforced AA6061 aluminum alloy produced by a conventional powder metallurgy technique, involving uniaxial cold

pressing and sintering of composite powders. Aluminum alloy with three different powder sizes were combined SiC particle with three sizes in various volume fractions up to 20% SiC. It is reported that the samples produced from the smaller aluminum powders exhibited reasonable UTS and modulus of elasticity with maximum values of 324 MPa and 104GPa, respectively.

X. Xia et. al. [11] investigated particle reinforced 2618, 7075 and 6061 aluminum alloys by three point bending tests. The results of the tests showed that for the same reinforcement volume fraction, the crack opening force is higher in 2618 and 7075 Al matrix composites due to the much higher levels of solute elements which causes matrix hardening. It is stated that the crack opening force is highest in 2618 composites because the matrix is strengthened by dispersoid particles and precipitates formed by overaging, whereas 7075 composites are weaker due to the absence of dispersoids.

Strengthening mechanisms for the dispersed particle-hardened RS composites include Orowan strengthening, grain size and substructure strengthening, and solid solution strengthening. Linear summation of such terms is often used to predict yield strength;

$$y = \sigma_{Orowan} + \sigma_{grain} + \sigma_{solute}$$

Orowan strengthening results from interactions between dislocations and the dispersed particles.

The flow stress of a material is almost universally observed to increase as the grain size decreases. The grain and substructure strengthening appears to be due to very fine grains via the Hall-Patch type of equation. [12]

When a foreign atom dissolves in the matrix it may act as an atomic sized obstacle to the motion of dislocations. If the foreign atom has a size different than the parent atoms, then a misfit strain field will be produced around the foreign atom that may interact with the dislocation stress field. [12]

2.3 Reinforcing Materials

Several materials such as oxides, carbides, nitrides, borides, sulfides, intermetallics, silicides may be used as reinforcement materials in metal matrix composites. [13]

Cost, elastic modulus, tensile strength, density, melting temperature, thermal stability, coefficient of thermal expansion, compatibility with matrix material, size and shape criteria are considered to select the ceramic reinforcements. [2]

Melting temperature of reinforcement is a good indicator of its usefulness for high temperature composites. Its importance results from the fact that it is considered to be the most useful structure insensitive property and it is related to many other properties, such as stiffness and stress values which both increase with melting point. It is also related to the thermal expansion coefficient which vary inversely with Tm. Melting points of reinforcements used for high temperature matrices are between 1500^oC and 3775^oC (NbC). Carbides have the highest melting points followed by nitrides, borides and oxides. [13]

In table 2.2, some selected properties of typical ceramic reinforcements are shown. [2]

Table 2.2 Selected Properties of Typical Ceramic Reinforcements [2]

Ceramic	Density (x10^{-3}kg m^{-3})	Expansivity (10^{-6} °C^{-1})	Strength (MPa)	Elastic Modulus (GPa)
Al$_2$O$_3$	3.98	7.92	221(1090°C)	379(1090°C)
C	2.18	-1.44	-	690
MgO	3.58	11.61	41(1090°C)	317(1090°C)
Si	2.33	3.06	-	112
SiC	3.21	5.40	-	324(1090°C)
SiO$_2$	2.66	<1.08	-	73
TiB$_2$	4.50	8.28	-	414(1090°C)
TiC	4.93	7.60	55(1090°C)	269(24°C)

The structural efficiency of discontinuously reinforced MMCs is affected by density, elastic modulus and tensile strength of the reinforcing phases. For the end application and during fabrication, chemical stability and compatibility of the reinforcement with the matrix is important. [2]

In normal instances, fine reinforcements and a relatively large volume fraction are preferred in order to increase strength and ductility. However it is difficult to take both advantages of these requirements because they are prone to cause an inhomogeneous distribution. Poor distribution of reinforcement degrades the composites in terms of its physical and mechanical properties. Figure 2.1 shows the ideally homogeneous distribution of spherical reinforcement [3]

2.4 Matrix Materials

Aluminum alloys are the mostly used matrices both in industrial applications and research studies for a long period of time. The main reason is low density. Moreover they are cheap if compared with other low density alloys such as Mg or Ti. Also, aluminum alloys are very well known due to their high use in several industries, from automotive to aeronautics. Their excellent behavior, from different points of view (strength, ductility, corrosion) can be modified in order to satisfy different applications. [3]

To use metal matrix composites for high temperature applications thermodynamically stable dispersoids are required. Due to this reason, an alloy-dispersoid system in which elemental solubility, solid state diffusivity and interfacial energies are minimized is preferred. This system minimizes coarsening and interfacial reactions. Alloying additions results in MMCs with attractive combinations of strength, ductility and toughness. [2]

For matrix powders, the final transverse length depends on the reduction ratio R and the original powder size d_m . The reduction ratio is the change of cross section area of the material before and after deformation. Approximately, each of the matrix powders is considered to experience the same deformation so that their cross-section

area change is consistent to the reduction ratio of bulk material R. By this consideration, the ratio of original transverse length d_m .and final transverse length d_f should be equal to the square root of the reduction ratio. [2]

2.5 Rapidly Solidified Aluminum Alloys

Rapid solidification is a way of forming amorphous or microcrystalline structures. The amorphous metals are glassy with a random, noncrystalline structure whereas microcrystalline materials possess a fine crystal size. Cooling rate determines the homogeneity, crystal size and degree of crystallinity. To obtain an amorphous structure, it is necessary to achieve cooling rates higher than 10^6K/s. [14]

Solid solution and precipitation strengthened aluminum alloys of series 2000, 5000, 7000 and 8000 use the advantages of rapid solidification: widely increased limits of solid solubility, very fine microstructure and lack of segregation. The other big group of RS alloys focused on dispersion hardening to provide usage at elevated temperature service conditions. Nearly all aluminum producers has made remarkable progress in dispersion strengthened alloy production: Alcan promotes AlCrMnZr, Alcoa favors AlFeCe, Pechiney AlFeMoZr, Allied Signal AlFeVSi, etc. [15]

Elevated temperature properties of these alloys are due to the thermally stable dispersoids in the microstructure. The requirements for such dispersoids are;

-the alloying element has high liquid solubility to have a large volume fraction of the dispersoid in the microstructure
-the alloying element should have low solid solubility and low diffusivity to have a minimal coarsening during high temperature exposure
-alloy should be solidified very rapidly to form the required dispersoids or their precursors on a fine scale and not to form coarse intermetallics. [16]

Solubility limit of Si in aluminum extends from a value of 1.6 %(at 850K under equilibrium) to 16% by rapid quenching. [14]

A very fine microstructure without segregations is obtained in RS alloys due to the completion of solidification in a very short time. Cooling rates up to 10^6K/s leading to undercooling of 100K widen the solubility gap .[15] Table 2.3 gives an idea of cooling rates of different rapid solidification techniques.[1]

Table 2.3 RS Techniques, Morphology and Cooling Rates [1]

Technique	Product Type	Typical Dimensions(μm)	Typical Cooling Rate(K/s)
Gas atomization	smooth, spherical powder	50-100	10^2-10^3
Water atomization	rough, irregular powder	75-200	10^2-10^4
USGA	smooth, spherical powder	10-50	$\leq 10^6$
PMRS	spherical powder	<1-50	$>10^6$

USGA, ultrasonic gas atomization; PMRS, plasma melt and rapid solidification. [1]

During atomization, spherodization and solidification occur. In general, by gas atomization spherical or nearly spherical shaped powder particles of aluminum alloys obtained. Tagstri et. al. [17] explained the irregularity of a powder shape as an indication of high rate solidification that the melt had insufficient time to complete spherodization. But Srivastava et. al. [23] claims that the sherodization time was always less than the time required by the droplets to attain the solid form during flight. They added that due to the collision with other coarse/fine droplets during flight, it is difficult for coarse droplets, which are in the liquid state for longer time as compared to fine droplets, to achieve spherical shape.

Powder atomized powders cooled by convection while ribbons cooled by conduction. The cooling rates are estimated by measuring secondary dendrite arm spacing. [15]

In their study, S.K. Das et. al. [18] showed that, superior mechanical properties of rapidly solidified aluminum alloys could retain their properties in large product

forms. For the large scale manufacturing of these alloys for aerospace structural applications; planar flow casting/ribbon communition, powder degassing and compaction processes are applied. The tensile properties of sheets made from various sizes of billets of rapidly solidified Al-Fe-V-Si alloy presented in table 2.4.

Table 2.4 Tensile Properties of Sheets Made from Various Sizes of Billets of Rapidly Solidified Al-Fe-V-Si High Temperature Aluminum alloy 8009 [18]

Billet size		Sheet size	Tensile Properties		
Diameter(mm)	Weight(kg)	(mm)	Y.S.(MPa)	U.T.S.(Mpa)	El %
115	3.2	2x125x203	430	454	13.3
279	68	2x610x1220	415	446	11.3
559	273	2x1372x2032	440	453	15.2

2.6. Rapidly Solidified Al-Fe-V-Si Alloy

Dispersion strengthened Al-Fe-V-Si quaternary alloy that has recently been developed using rapid solidification techniques, has attracted interest because of its high strength at elevated temperatures. The reason of this high elevated temperature strength is the establishment of a cubic silicide phase as an intermetallic phase, when the alloy is rapidly solidified. [5].

The addition of a quaternary element to Al-Fe-Si alloy system to stabilize the cubic α-$Al_{12}Fe_3Si$ phase which is a metastable intermetallic was studied by Skinner et. al. [19]. They concluded that addition of vanadium to the system stabilizes $Al_{12}(Fe, V)_3Si$ phase rather than equilibrium hexagonal Al_8Fe_2Si phase. $Al_{12}(Fe,V)_3Si$ has a complex bcc cubic structure having 138 atoms/unit cell which is isostructural with $Al_{15}Mn_3Si_2$.

Commercial Al-Fe-V-Si alloys; FVS 0611, FVS 0812(also named as 8009 alloy) and FVS1212 are produced by Allied Signal Inc. with compositions 6.5%Fe-0.6%V-1.3%Si, 8.5%Fe-1.3%V-1.7%Si, 12.4%Fe-1.2%V-2.3%Si and dispersoid volume fraction of 16%, 24%, 37% respectively. The alloy is formed by rapid solidification

using melt spinning techniques, followed by comminution and subsequent powder compaction by extrusion between 375°C and 425°C [20, 21].

2.6.1 Microstructure of Al-Fe-V-Si Alloy

Microstructure of gas-atomized powders of Al-Fe-V-Si consists of several forms of icosahedral phase distributed in either supersaturated solid solution of α-Al matrix, or in intercellular/dendritic regions depending on powder particle size. [22]

Several metastable and stable phases develop by rapid quenching of quaternary Al-Fe-V-Si alloys. A small fluctuation in solidification time and composition favors the transition from icosahedral quasicyrstalline phase to a crystalline phase or vice versa during processing. In table 5, commonly occurring phases, their morphology and crystal structure is shown. [23]

Table 2.5 commonly occurring phases, their morphology and crystal structure of Al-Fe-V-Si alloy [23]

Phase	Morphology	Crystal System
i-Al(Fe,V)Si	Round grains, star shaped	icosahedral
α-$Al_{12-14}(Fe,V)_3 Si_{1-2}$	spherical	cubic
$(Al,Si)_{13} Fe_4$	band shaped	monoclinic
θ-$Al_2(Fe,V,Si)$	polygonal	hcp

Tagsri et al. [24] examined powders of the alloy Al-6.5Fe-1.5V and Al-6.5Fe-1.5V-1.7Si which had been produced by gas atomization technique. The microstructures depended on powder particle size. In fine particles(<5μm) ultra fine microstructures which consisted of ultra fine, discrete rounded particles with diameters less than 50nm distributed throughout the α-Al matrix were observed and named as zone A. The formation of this zone is due to advancing planar α-Al into the melt and engulfing the ultra fine dispersed MI (microquasi crystalline) particles. In medium sized powders (5-15μm) the planar front was not stable at velocities below the absolute velocity and turns into cellular front. The freely dispersed MI phase

particles pushed laterally by the cellular front and entrapped in the intercellular liquid that solidifies later at the end of the solidification of a melt droplet. This microstructure is named as B and may exist with zone A depending on the powder size. Microstructure of coarse powders consists of zone B and zone C. In zone C, the cellular α-Al front changed to a dendritic mode. The dispersed phase in zone C was reported as, either icosahedral phase or globular cluster of randomly oriented MI phase. The globular particles are as large as the cellular or primary dendrite arm spacing so they were not trapped in the intercellular/interdentritic regions, instead they were stuck to coarse cellular/dendritic networks.

Park et. al. [25] investigated melt spun ribbons of Al-8.5 Fe-1.3 V-1.7Si alloy which had different microstructures varying due to the casting conditions and thickness of the ribbon. They examined two microstructures; zone A consisting of fine particles in Al matrix and the mixed zone (zoneA+zoneB) with much more discrete fine particles shown in the optical micrographs, figure 2.2.
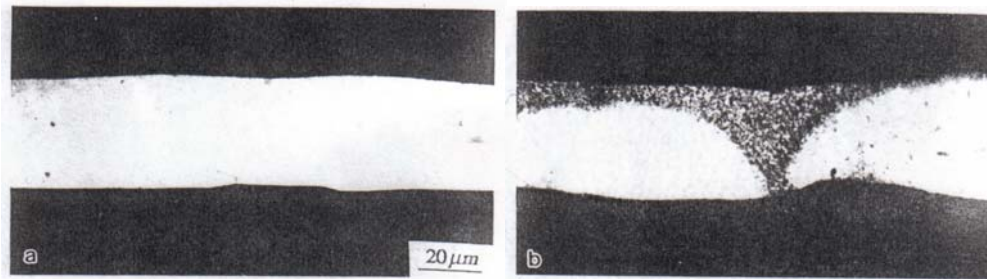

Figure 2.2. Optical micrographs of a) zone A b) mixed zone [25]

Park et al. [25] reported that the microstructure of the completely zone A ribbon consisted of the microcellular precipitation of microquasi crystalline phase, with globular particles of clustered microquasi crystalline phase near the air side of the ribbon. In the ribbons with mixed zone, intercellular phase composed of silicide phase (which can be indexed as $Al_{12}(Fe,V)_3Si$) and also globular particles of microquasi crystalline phase near the air side. The globular phase in zone A ribbon composed of only microquasi crystalline phase while globular particles in the mixed ribbon

consisted of microquasi crystalline phase and silicide phase. This silicide phase had transformed from the microquasi crystalline phase because of recalescence. After annealing at 400°C for 4 hours, the microstructure of the A ribbon is much coarser than the mixed ribbon. In zone A, intercellular microquasi crystalline phase particles transformed into coarse silicide particles and silicide particles located along the matrix –globular particle interface consume the globular particles and coarsen at a very fast rate. In mixed zone, the original shape of the particles disappeared and final appearance resembled coarse cellular structure with new intercellular silicide particles formed from the decomposition of the globular particles. Park et. al. reported that, in contrast to the general belief, the ideal microstructure in the rapidly solidified alloy is certainly not the completely zone A structure, owing to the thermal instability of the microquasi crystalline phase.

Wang et. al. [26] studied on the microstructural stability of melt-spun ribbons of Al-13.4Fe-0.85V-2.23Si alloy, produced by planar flow casting solidification processes. The ribbon was reported to be 20-40μm thick and 20mm wide. Microstructure of the ribbon characterized by fine grains and nearly spherical precipitates with a size of 50nm. The precipitate was indexed as b.c.c α-Al_{13}(Fe,V)$_3$Si phase mainly distributed along grain boundaries forming particle clusters. The good properties of the alloy were due to the homogenous distribution of these fine dispersoids which improve the temperature of recrystallization and resist the growth of grains. They stated that no noticeable growth of dispersoids observed up to 510°C for 100 hours. The examination of the specimens which had been exposed to 650°C for 25 hours showed that new vanadium free hexagonal θ-$(Al,Si)_{13}Fe_4$ phase existed in the form of a band. They explained the reason of this transformation by the enhanced diffusivity of V atoms by high temperature. The growth rate of the $(Al,Si)_{13}Fe_4$ phase was four to five orders of magnitude higher than that of nearly spherical $(Al,Si)_{13}Fe_4$ phase.

Kalkanlı et. al. [27] investigated an Al-8.4Fe-1.6V-2.5Si alloy produced by gas atomization and spray deposition. Gas atomized powders were deposited on a water cooled rotating copper substrate. They observed a layered structure which is detrimental to the mechanical properties in the middle of the preform, figure.2.3 and

figure 2.4. The layer was due to the transient liquid phase formation and segregation of Fe, Si and V during solute rejection. Point analysis of the dark and white area gave Al-0.05Si-00Fe-0.49V and Al-6.06Si-13.7Fe-2.00V respectively. The dark area was nearly single phase Al, while there was an increase in the amount of the cubic phase in white layer.
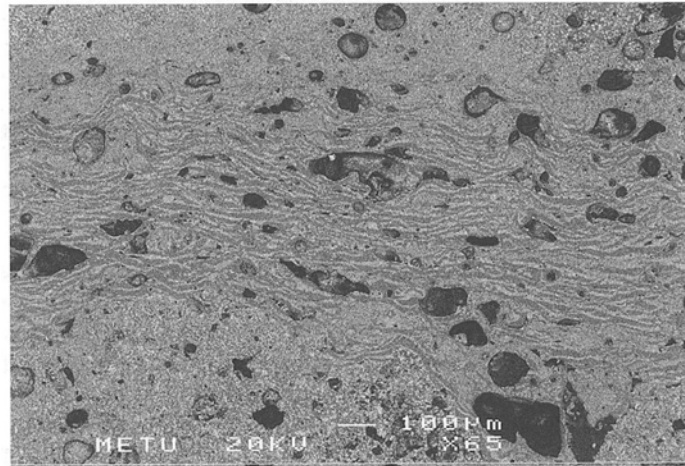

Figure 2.3 Backscattered image of spray deposited Al-Fe-V-Si alloy containing layered zones, in the middle, and some pores (black areas) and fine dispersoid rich zone at top and bottom. [27]
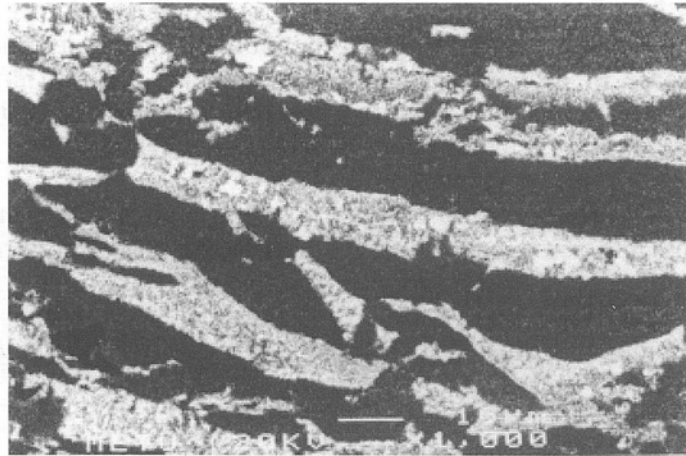

Figure 2.4 Layered structure observed at cross section of deposited perform [27]

Extruded samples produced from fine (<15mμ) gas atomized powders of Al-6.5Fe-1.5V-1.7Si alloy exhibited microstructures consisting of ultra fine spherical-like particles distributed homogeneously throughout the α-Al matrix. Banded structures

14

was observed for the extrudates produced from coarse powders. Microstructures of the extrudates are presented in figure 2.5 and 2.6.[22]
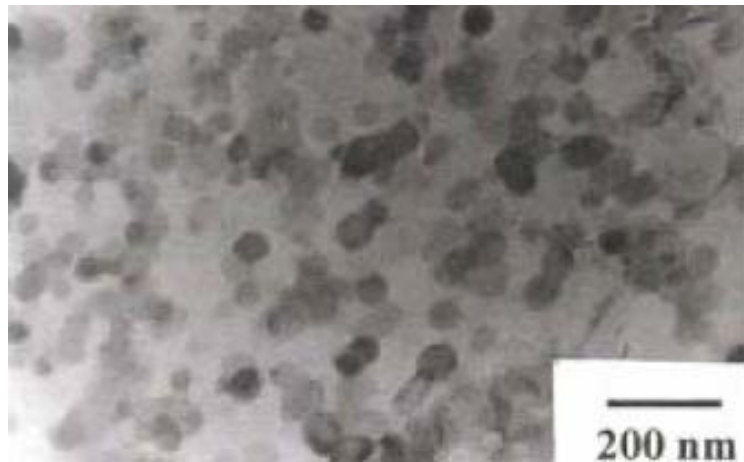

Figure. 2.5 TEM micrograph of the microstructure of the extrudate produced from fine powder particles [22]

Figure 2.6. TEM micrograph of the microstructure of the extrudate produced from coarse powder particles [22]

The banded structure in figure 2.6. consisted of a band with a high volume fraction of ultra fine silicide particles parallel to a band with low volume fraction of coarse silicide particles.

In the study of Franck et. al. [21] the microstructural stability of AlFeVSi alloy was assessed. Extruded samples of FVS1212 annealed at 500ºC, 550ºC and 600ºC for

1000hours were examined. Annealing at 500ºC for 100 hours caused a few grains to coarsen from 470 nm to 1µm and dispersoids to coalescence into clusters, figure 2.7 and figure 2.8
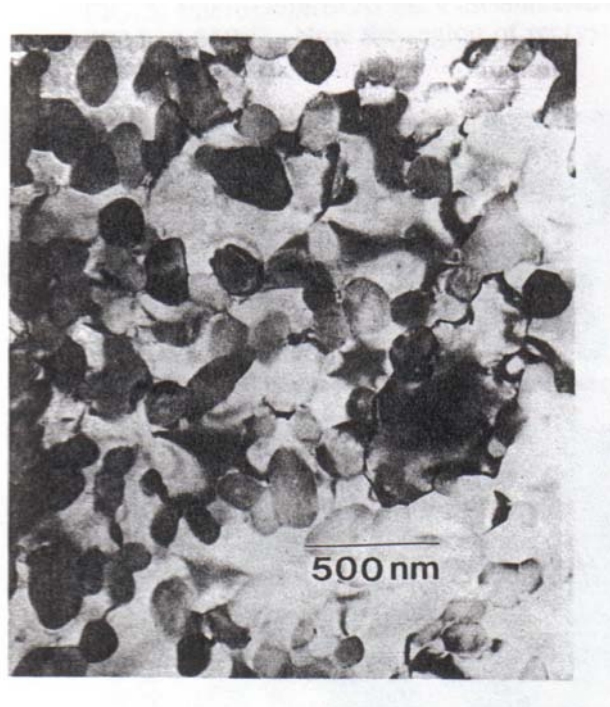

Figure 2.7.Microstructure of extruded samples of FVS1212 alloy as received [21]
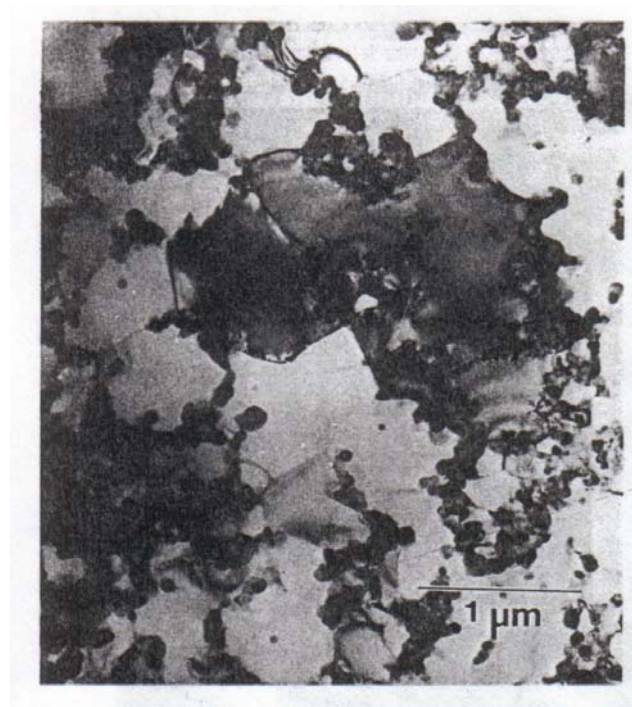

Figure.2.8 Microstructure of extruded samples of FVS1212 alloy after annealing for 100h at 500ºC. [21]

Franck et. al. [21] observed that grain growth and particle coarsening proceeds more rapidly when samples were annealed at 550ºC. After 10 hours grain growth occurs, α-Al$_{12}$(Fe,V)$_3$Si particles along the grain boundaries coarsen and form a necklace structure due to the enhance diffusion along the grain boundary. After 500h at 550ºC, recrystallized grains were seen with the grains elongated in the extrusion direction, figure 2.9. After annealing at 600ºC for 10h, parallel regions of recrystallized matrix were observed, fig 2.10.

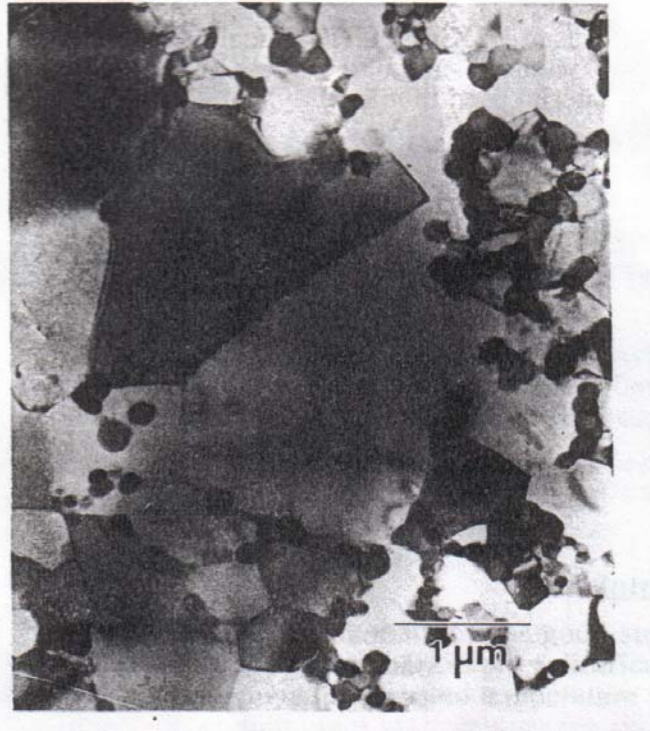Figure 2.9.Microstructure of extruded samples of FVS1212 alloy after annealing 500h at 550ºC. [21]

Figure 2.10 Microstructure of extruded samples of FVS1212 alloy after annealing 600ºC for 10h. [21]

2.6.2. Mechanical Properties of AlFeVSi Alloy

The improved elevated temperature strength and stability of the alloy is attributed to the slower coarsening rate of the silicide particles, about $10^{-27} m^3/h$. [18, 19]. Also, high volume fraction of dispersoids inhibit recrystallization and grain growth to a certain extent and limit losses due to the long term high temperature annealing treatments. [21]

Mitra et al. [28] presented engineering stress/strain curves of FVS 1212 obtained at various temperatures from 25ºC to 350ºC, figure 2.11. While the yield strength decreases normally with increasing test temperature, the extent and the rate of the subsequent strain hardening showed a maximum at intermediate temperatures.
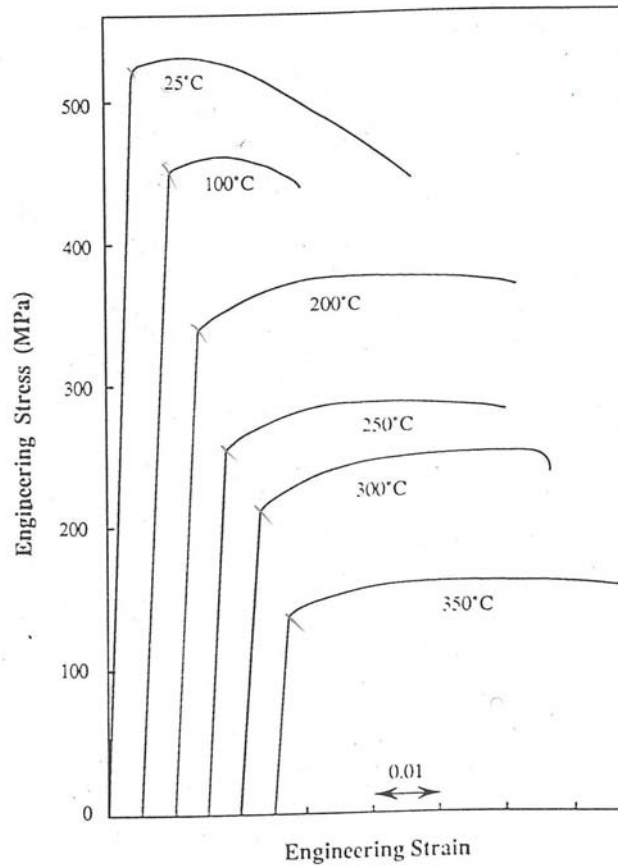
Figure 2.11 Engineering stress/strain curves of FVS 1212 obtained at various temperatures from 25ºC to 350ºC[28]

Franck et al. [21] also assessed mechanical properties of FVS1212 alloy produced by extrusion. The average values of room temperature UTS and yield strength were 512±8 MPa and 488±5 MPa, respectively. There was no change in the hardness of the alloy after annealing at 500ºC for 100 hours, while overall reduction of 22.5 pct was observed after annealing 1000 hours at 550ºC. The alloy showed a decrease in tensile strength only after annealing 100 hours at 500ºC. Hardness and tensile strength vs. annealing temperature is presented in figure 2.12 and 2.13.
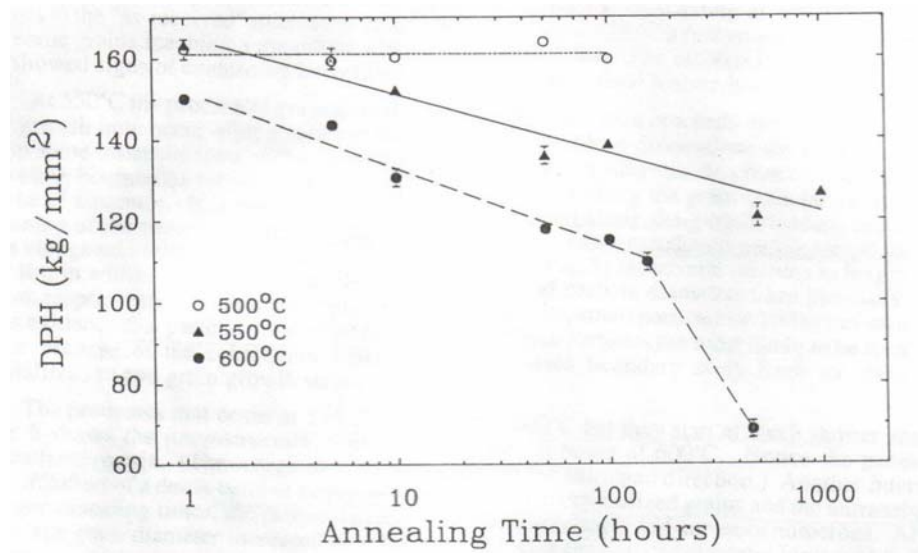
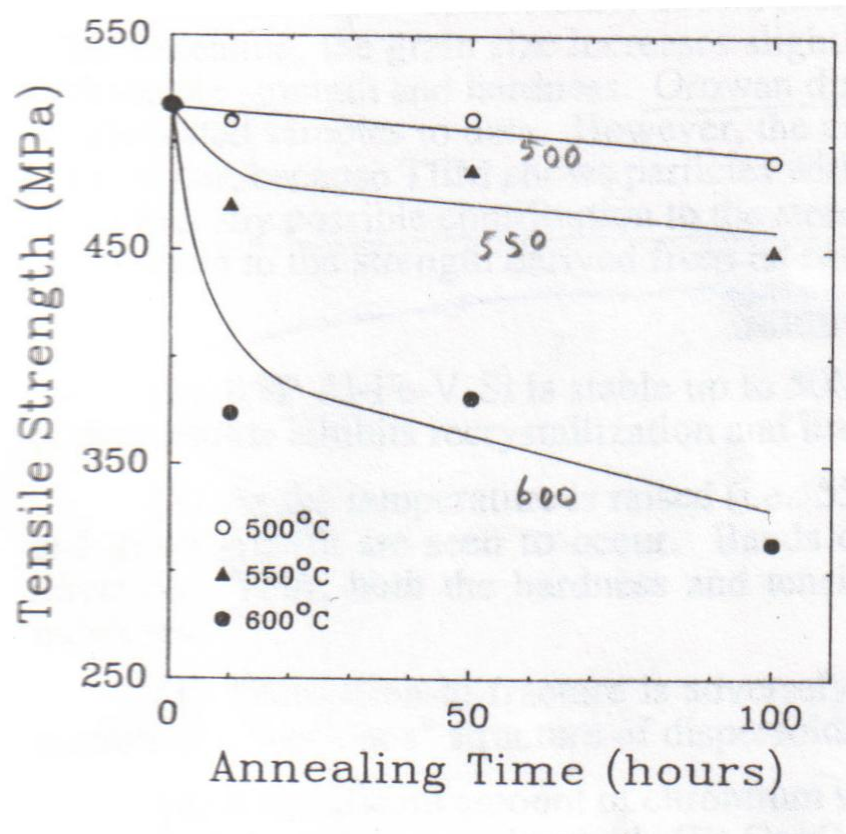Figure 2.12 Hardness vs. annealing temperature of FVS1212 alloy [21]

Figure 2.13 Tensile strength vs. annealing temperature of FVS1212 alloy [21]

Decrease in tensile strength and hardness can be attributed to the recovery and recrystallization of the aluminum matrix while decrease in ductility can be traced to the agglomeration of particles along the grain boundaries. [21]

20

Lee et al. [29] identified embrittlement behavior of RS PM Al-Fe-V-Si alloy with a composition of Al-8.5Fe-1.3V-1.7Si after high temperature exposure at 480°C for 100 h. The specimens used were produced by extrusion. The alloy was compared to an ingot metallurgy 2219 aluminum alloy and the results of this comparison exists in the table 2.6

Table 2.6. Comparison of mechanical properties of 2219 aluminum alloy and RS PM Al-Fe-V-Si alloy[29]

Alloy	Yield strength(MPa)			Elongation (%)			Fracture toughness(MPam$^{1/2}$)		
	As rec.	430°C	480°C	As rec.	430°C	480°C	As rec.	430°C	480°C
AlFeVSi	353	359	314	16.1	14.8	7.8	34.9	30.8	16.1
2219T811	354	66	-	12.9	29.0	-	34.9	-	-

As it is seen from table 2.6 RS PM Al-Fe-V-Si alloy showed excellent stability compared to the 2219 aluminum alloy but there is a decrease in fracture toughness, ductility and yield strength after high temperature exposure. In their investigation Lee et al. [29] decided that the decrease in these mechanical properties were due to the formation of coarse needle shaped monoclinic θ-$Al_{13}Fe_4$ particles and presence of this particle might limit the upper service temperature of the alloy.

The precipitation of coarse $Al_{13}Fe_4$ was also reported by R. Hambleton et al. [30]. The change had occurred in the microstructure of unreinforced Al–Fe–V–Si after 100 h at 550ºC, figure 2.14.
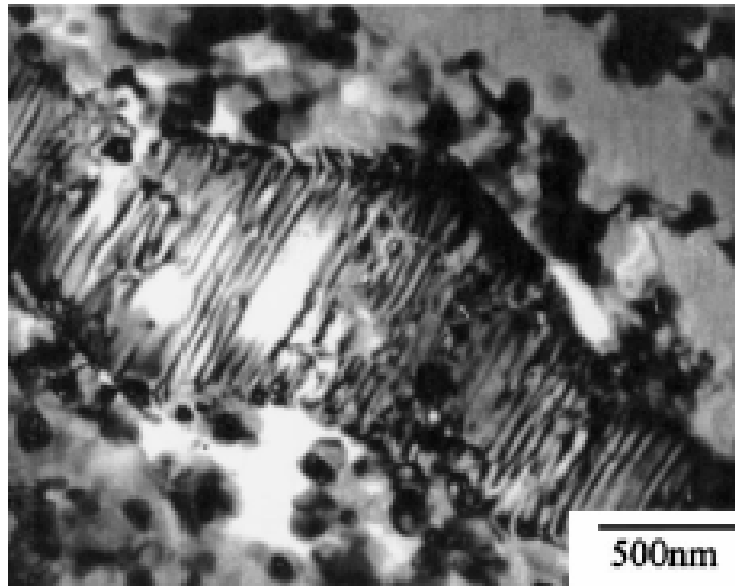
Figure 2.14 TEM micrograph of precipitation of $Al_{13}Fe_4$ in Al–Fe–V–Si after 100 h at 550ºC [30]

From the fractographs of tensile specimens of AlFeVSi alloy it was observed that a ductile dimpled rupture existed in as received and high temperature exposure cases, however, some areas of brittle cleavage-like fracture had occurred in the specimen exposed to 480°C. [29]

Compressive strength of extrudates produced from fine powder of AlFeVSi alloy is high at room temperature due to the existence of ultra fine spherical like particles whereas extrudates produced from coarse powder of AlFeVSi alloy is low due to the banded structure. [22] Compressive strength vs. powder particle size is presented in figure 2.15.
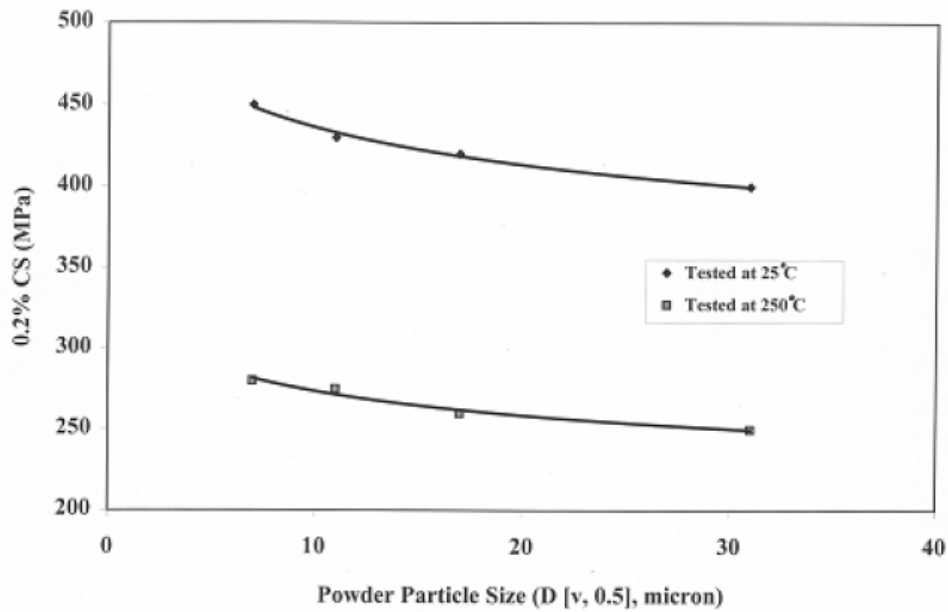
Figure 2.15 Compressive strength of the extrudates [22]

2.6.3 Al-Fe-V-Si Alloy Based Composites

Radmilovic et. al. [31] examined the microstructure of a monolithic AlFeVSi alloy and SiC particulate composite based on this alloy. The MMC specimens were produced by extrusion and hot rolling. It consists of $Al_{13}(Fe,V)_3Si$ silicide particles in the α- Al solid solution matrix. The silicide particle size was in the range 20 and 100nm. There was a tendency of silicides to form agglomerates due to the fact that silicides are located at the cell boundaries during rapid solidification. The grain size is in the range 0.5-0.2 μm. The microstructure of the monolithic Al-Fe-V-Si alloy is presented in figure 2.16.
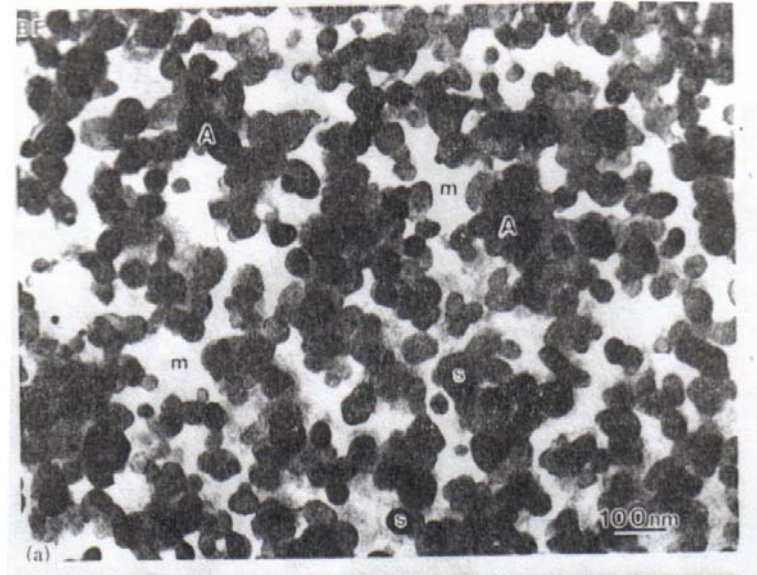
Figure. 2.16 Microstructure of the as extruded monolithic Al-Fe-V-Si alloy [31]

The typical structures of as extruded and hot rolled metal matrix composites in the study of Radmilovic et. al. [31] are shown in figure 2.17 and 2.18. It consists of SiC particles (p) and silicide particles(s) in α- Al matrix. SiC particle size is same in both extruded and hot rolled samples, 0.5-5 μm. In hot rolled MMC the silicide particle size is greater, in the range of 50-200nm.
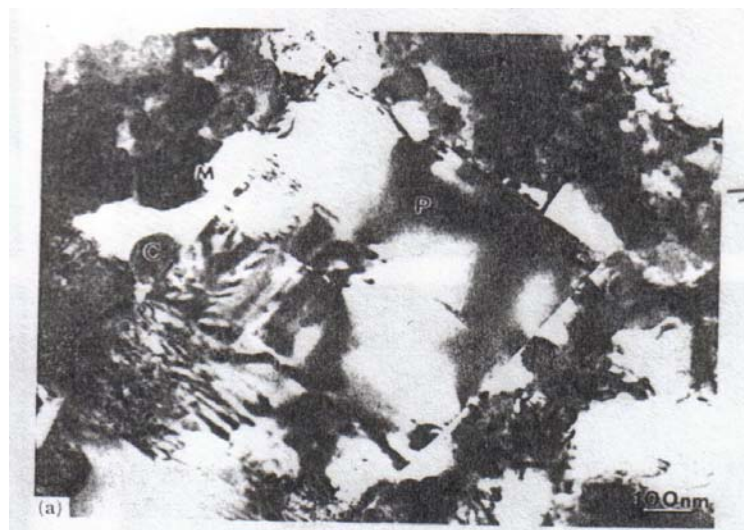

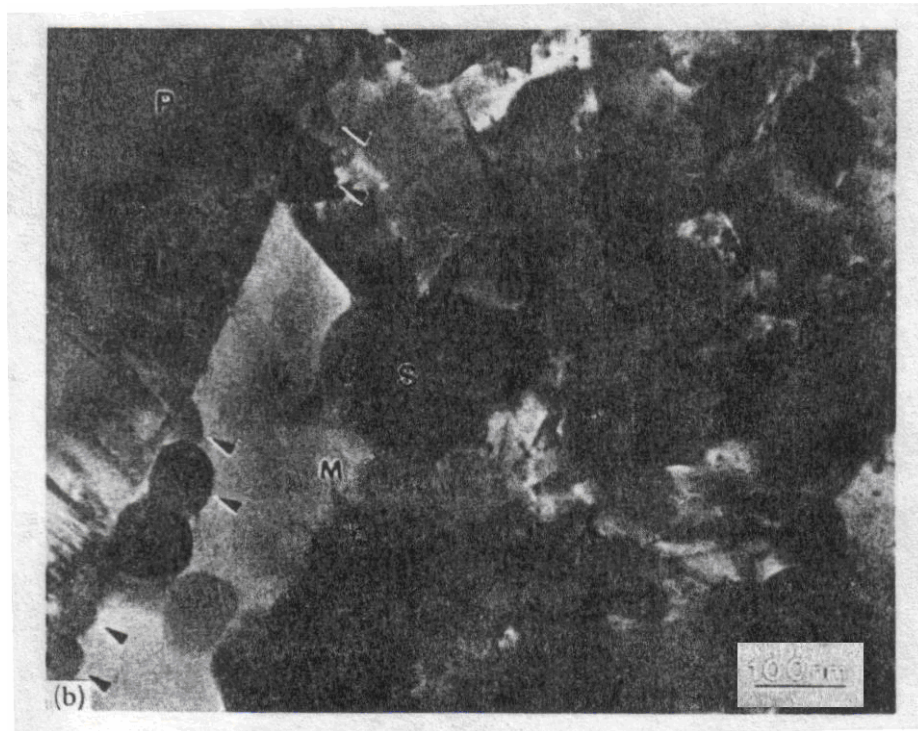Figure. 2.17 As extruded metal matrix composites [31]

24

Figure 2.18 As extruded metal matrix composites [31]

Radmilovic et. al. [31] observed that SiC changed abruptly from the 6H polytype structure in a very narrow region next to the α-Al-SiC interface. This was an indication of a change in composition. The change in composition was due to diffusion of a very limited amount of silicon and carbide into the α-Al since from the ternary phase diagram it was assumed that there was no solubility of aluminum, iron and vanadium in SiC. Therefore, the interfacial reaction layer is very narrow and the driving force for this reaction is such as to lower the free energy of the interface.

Hambleton et al.[30] studied the effects of variable matrix alloy composition and reinforcement with 20 wt% SiC on the response to exposure at 425ºC and 550ºC of rapidly solidified Al–8.3Mn–2.9Si, Al–9.8Mn–3.0Si and Al-8.3Si–1.3V–1.7Si alloys, prealloyed, argon atomized and mechanically milled prior to consolidation by forging at 495ºC. Figure 2.19 shows the microstructure of reinforced Al-8.3Si–1.3V–1.7Si alloy.
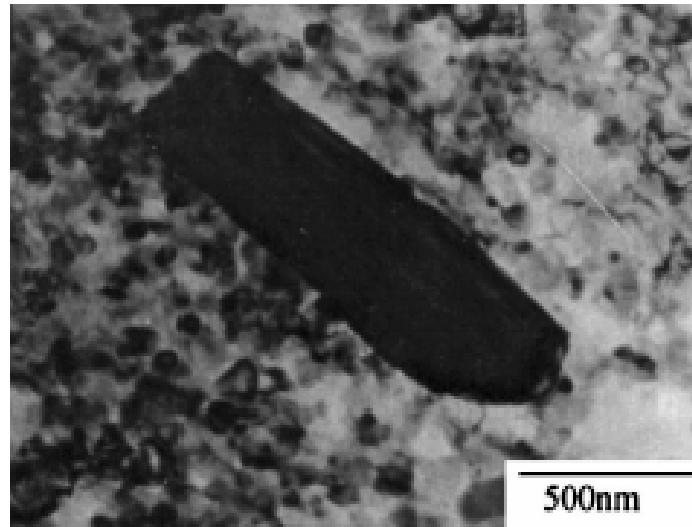
Figure 2.19 TEM micrograph of a typical SiC particle (size 1 to 3 mm) and fine silicides in Al–Fe–V–Si alloy [30]

Hambleton et al. [28] stated that precipitation of coarse $Al_{13}Fe_4$ had occurred in the microstructure of unreinforced Al–Fe–V–Si after 100 h at 550ºC while the formation of $Al_{13}Fe_4$ was not detected in the reinforced Al–Fe–V–Si even after further treatment for 100 h at 600ºC; although, precipitation of Al_4C_3 resulted by partial dissolution of SiC was detected, figure 2.20 [30].

Figure 2.20.TEM micrograph of precipitation of Al_4C_3 (arrowed) in reinforced Al–Fe–V–Si after 100 h at 550ºC. [30]

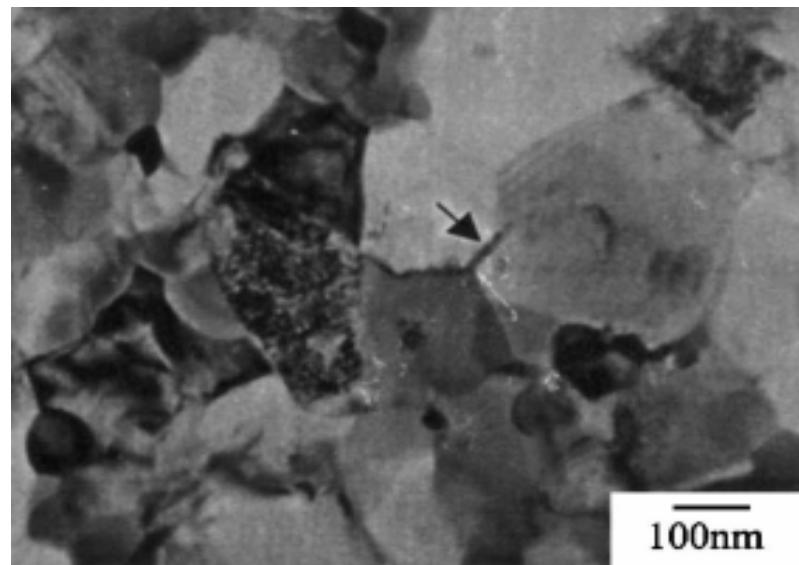Mechanical properties of forged specimens in Hambleton et al.'s [30] study presented in table 2.7 and 2.8.

Table 2.7 Vickers hardness (kg/mm2) both as-forged and after heat treatment at 425 or 550ºC[30]

Condition	Unreinforced Al–Fe–V–Si	+20SiC
As-forged	139±1	191±2
100 h/425ºC	141±1	-
1000 h/425ºC	141±1	-
3100 h/425ºC	107±1	-
100 h/550ºC	134±1	174±1

Table 2.8 Tensile properties at 20ºC and 350ºC[30]

Condition Tested at 20ºC:	Unreinforced Al–Fe–V–Si	+20SiC
UTS (MPa)	491±5	395
$\sigma_{0.2}$ (MPa)	350±4	-
ε_f(%)	1.9±0.1	0.6
Tested at 350ºC	Unreinforced Al–Fe–V–Si	+20SiC
UTS (MPa)	190±10	172
$\sigma_{0.2}$ (MPa)	157±8	166
ε_f(%)	5.5±0.4	-

2.6.4. Commercial Production of Al-Fe-V-Si Alloy

Allied Signal maintained a leadership position in the production of AlFeVSi alloy by planar flow casting. Molten metal is directed through a slotted nozzle onto a rapidly moving, water cooled casting substrate. Upon contact with the chill surface, the alloy experiences cooling rates of up to 10^6K/s and undergoes significant undercooling before solidifying into ribbons. The advantage of the process is that the

ribbon has uniform structure. The structure and properties of powder are therefore independent of particle size and powder yield is 100%. [15, 18]

The RS aluminum alloy ribbons are reduced to powder by a series of mechanical milling process. The ribbon coming off the casting wheel is conveyed into a mill reduced into shards. A second mill reduces the shards to the final powder product that is sieved and stored in powder storage and transfer vessels. The powder size for billet fabrication is -40 meshes in size, +40 meshes are reprocessed. Billets are produced by canning the powder and evacuated and heated for degassing. The sealed cans are heated and compacted to near full density with a pressure of 1600 tones, after which the can is machined away to produce a billet suitable for extrusion or forging. The company also produces Al-Li alloy by a similar process. [18]. The production steps are shown in figure 2.21
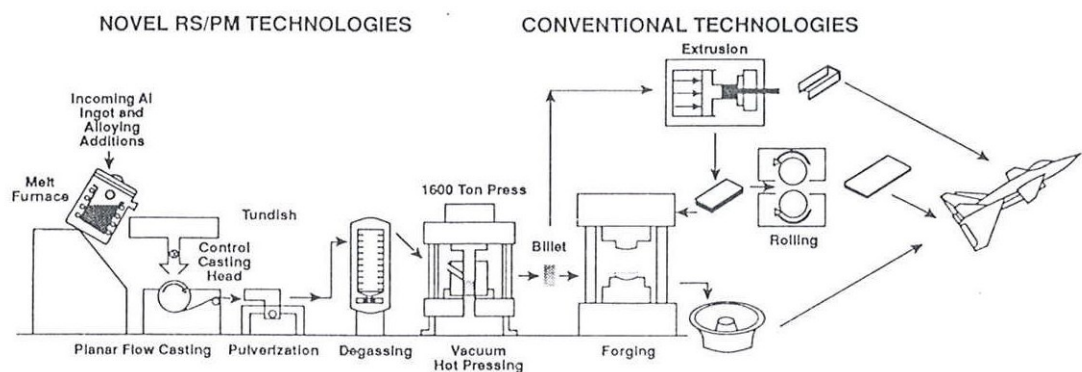

Figure.2.21.Shematic diagram of manufacturing process, as practiced by Allied-Signal. Inc. for RS aluminum alloys using combination of novel rapid solidification powder metallurgy process and conventional metal working technologies. [18].

2.7 Processing of Metal Matrix Composites

A variety of processes have been applied for the production of metal matrix composites in order to optimize the structure and properties. These processes can be grouped as;

-liquid state processes
-two phase (solid-liquid) processes
-solid state processes

2.7.1 Liquid State Processes

Liquid state processes are liquid metal-ceramic particulate mixing, melt infiltration and melt oxidation. Agglomeration of ceramic particulates during agitation, settling of particulates, segregation of secondary phases in the metallic matrix, extensive interfacial reactions and particulate fracture during mechanical agitation are the difficulties of liquid metal-ceramic particulate mixing. In melt infiltration process, a molten alloy is introduced into a porous preform, utilizing either inert gas or mechanical device as a pressurizing medium. Some drawbacks of melt infiltration are reinforcement damage, preform compression, microstructural nonuniformity, and coarse grain size. Melt oxidation process is used to obtain complex, fully dense composite shapes. A preform is infiltrated by a molten alloy as it undergoes an oxidation reaction with a gas phase. [2]

2.7.2 Two Phase (Solid-Liquid) Processes

Two phase processes are osprey deposition, rheocasting, and variable co-deposition of multi-phase materials (VCM). In osprey process, the reinforcement particulates are introduced into the stream of molten alloy which is subsequently atomized by jets of inert gas. The sprayed mixture is collected on a substrate in the form of a reinforced metal matrix billet. This process combines the blending and consolidation steps of PM process. In rheocasting, the ceramic particulates are added into a metallic alloy matrix at a temperature within the solid-liquid range of the alloy. The

ceramic particulates are mechanically entrapped initially and are prevented from agglomeration by the presence of primary alloy solid particles. During VCM processing, the matrix material is disintegrated into a fine dispersion of droplets using high velocity gas jets. [2]

2.7.3 Solid State Processes

Solid state processes include powder metallurgy (PM), diffusion bonding and high energy high rate processes. [2, 30] The production of MMPCs using modern high – performance materials such as tungsten, molybdenum, niobium and tantalum as the metal matrix is difficult by conventional liquid metallurgy techniques owing to the high temperatures involved. In such cases powder metallurgy with near net shape capability is more attractive. PM route also reduces the forming and machining cost correspondingly. [1] High energy high rate processes involve consolidation of a metal-ceramic mixture through the application of a high energy in a short period of time. This process has been successfully applied to manufacture Al-SiC and (Ti$_3$Al+Nb)-SiC composites. The maximum thickness that can be processed using commercially available energy sources is a subject to work extensively to access potential application of the process. [2] Diffusion bonding can be applied by a hot processing method. For example, anodized and unanodized Al foils hot rolled to generate a selected range of alumina volume fraction. Anodization of Al increased the thickness of alumina layer. [32]

2.7.3.1 Powder Metallurgy Processing

Powder metallurgy route has some advantages over ingot metallurgy or diffusion welding such as;

 - The uniformity of reinforcement distribution improves the structural properties and reproducibility level in the properties.
- Strong interfacial reaction causing undesired reactions between matrix and the reinforcement is avoided by low manufacturing temperature

- Any material that cannot be produced by any other alternative route can be produced by powder metallurgy technique, i.e. Ti alloys reinforced with SiC.
- Particle or whisker reinforced composites can be easily produced by P/M. [4]

P/M aluminum matrix composites present good mechanical properties when compared with those produced by other techniques. [6]

In powder metallurgy, conventional method for manufacturing includes blending or mixing, followed by compaction and solid state sintering. [1] This means using lower temperatures than other alternative processing methods with less interaction between the matrix and reinforcement. [4] These processes are known as primary manufacturing. Further deformation of the PM products by extrusion, rolling or other hot working methods are named as secondary manufacturing. [1] A flowchart of such a fabrication process is given in figure 2.20. [2]

Ceramic reinforcement

↓

Deagglomaration   Metal Powder

Mixing and Degassing

↓

Billet Consolidation

↓

Scalping

↓

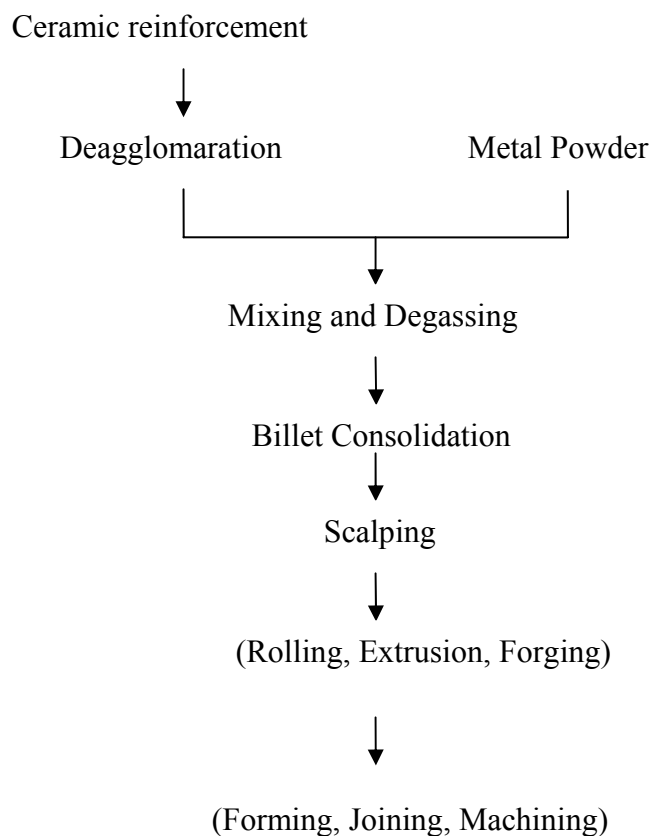(Rolling, Extrusion, Forging)

↓

(Forming, Joining, Machining)

Figure 2.20 PM MMC Fabrication Steps[2]

Theoretically, when secondary processing with a large enough deformation is introduced, a homogeneous distribution of reinforcements could be achieved regardless of the size difference between matrix and powder reinforcement particle. Unfortunately, the final size should ideally be net product, or near net product, thus reduction ratio in secondary deformation is limited. . [3]

2.7.3.1.1 Blending or mixing

Blending or mixing is important since it controls the final distribution of the reinforcement particle and porosity in green compacts after compaction, which strongly effects the mechanical properties of PM materials used. [1]

Mixing efficiency is determined by the volume of the powder in the mixer. A powder volume between 20% and 40% of the mixer capacity is usually optimal. Also, mixer operating conditions plays an important role. At low rotational speed is inefficient because of little motion while at high rotational speeds centrifugal forces can prevent mixing. [14]

2.7.3.1.2 Cold Compaction

Cold compaction of the powders at an appropriate pressure is done in order to obtain adhesion of powders to each other at room temperature. In conventional method of compaction, pressure is applied in one direction which may cause an uneven distribution of consolidation and insufficient densities. Cold, warm or hot isostatic pressing can provide better quality green compacts. [1]

The compaction of powders involves both rearrangement and deformation of the particles, leading to the interparticle bonds. The initial transition with pressurization is from a loose array of particles to a closer packing. Subsequently, the point contacts deform as the pressure increases. Finally, the particles undergo extensive plastic deformation. High pressures increase density by contact enlargement through plastic deformation. During deformation, cold welding at the interparticle contacts

contributes to the development of strength in the compact. As the compaction pressure further increased, the amount of each particle undergoing plastic deformation increases. At very high compaction pressures, in excess of 1Gpa, massive deformation occurs; continual pressurization beyond this level is of little benefit. The material response is similar to that of a dense solid. [14]

The pressures necessary to give satisfactory pressed components varies between fifteen and fifty tons/in^2 (232MPa-775MPa). Lower pressures give fragile compacts, while loads higher than fifty tons/in^2 cause tool distortion and breakage, high ejection pressures and rapid wear of the tools thus reducing their usual life. [33]

The height to diameter ratio is important to obtain uniform compact properties. Generally, when the height to diameter ratio exceeds five, die compaction is unsuccessful. [14]

A fine particle size hinders compaction because of the higher interparticle friction. Interparticle friction aids homogeneity in the pressing operation but hinders compaction by requiring much larger pressures. Thus, the effect of a high interparticle friction is to lower overall compact density while increasing homogeneity. [14]

2.7.3.1.3 Sintering and Other Consolidation Methods

The green compacts are usually sintered after compaction. [1] Packed metal powders bond together when heated to temperatures in excess of approximately half the absolute melting temperature. On a microstructural scale, cohesion takes place as necks grow at the point of contact. The reason for sintering is the energy excess associated with the surface area of unsintered metal powders. The motion of an atom is favorable since it reduces the net surface energy by decreasing the total surface area. The surface energy per unit volume depends on the particle diameter, thus finer particle sizes increase the driving force. However; not all the surface energy is available as a driving force. At every sintering interface there is the subsequent

creation of a grain boundary with associated grain boundary energy. Therefore, the net driving force can be quite small, and sintering can be sluggish. [14]

When two particles are in contact with, the microstructure changes as the bond between particles grows. This change is shown in figure 2.21. [14]

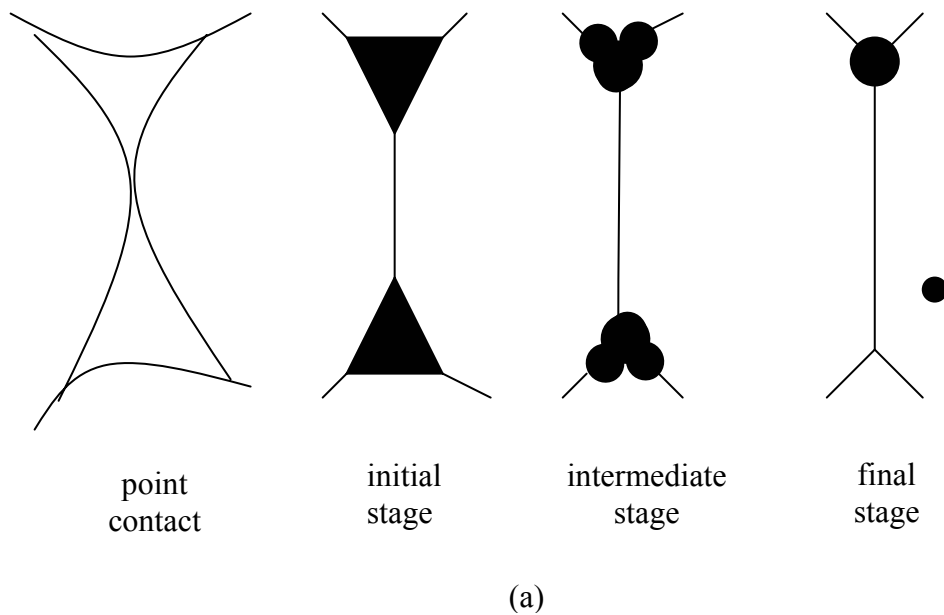| point contact | initial stage | intermediate stage | final stage |

(a)

(b)

Fig. 2.21a) The development of the interparticle bond during sintering, starting with a point contact. The pore volume shrinks and the pores become smoother. As pore sherodization occurs, the pores are replaced with grain boundaries. [14] b) sintered product with pores at powder boundaries.

The controllable parameters in sintering are the sintering temperature and atmosphere. Commonly occurring problems are the presence of oxide films, imperfect distribution of particles and sweating during liquid phase sintering and poor strength in solid phase sintering. [1]

Sometimes other consolidation methods can be applied as;

-Hot pressing
-High Energy High Rate Processing
-Resistance Sintering
-Dynamic Consolidation

Three concerns in discussing hot pressing of powders are temperature, stress and strain. Full density is ineffective at temperatures below approximately one half of the melting temperature. Temperatures between 70 and 85% of the absolute melting temperatures are optimal. In hot consolidation, the effective stress is the stress at the interparticle contacts which differs from the external stress because pores act as stress concentrators. The third variable strain tends to promote less ductility if it is high and fracture is more likely. Alternatively, a low strain rate provides more plastic deformation of the compact with a higher final density. [14]

Dynamic consolidation is a more recently developed technique to produce materials using rapidly solidified or amorphous-structured powders. This method consists of using explosives or a high velocity punch to impact the powders, causing instantaneous compaction. The advantages of this method are relatively low bulk temperatures, nearly random crystallographic texture in the final products, and shock hardening. A shock wave can be introduced in three ways;

A propellant or compressed gas in a gas gun
By direct application of explosives
By the impact of a projectile accelerated by explosives.

Much higher pressures and interparticle melting during shocking result in almost full densification. [1]

Swaging is a process for reducing the diameter, tapering or pointing round bars or tubes by external hammering. A useful extension of the process involves the formation of internal cavities. Here, a shaped mandrel is inserted inside a tube, and the tube is then collapsed around it by swaging. [34]

Swaging is done by means of a rotary machine, as shown in figure 2.22 and 2.23. Rotation of the spindle within the cage causes the backer blocks to alternately move apart and then be forced inward to pass beneath the rollers. The dies then open and close from various angles around the workpiece. The operator inserts the bar or tube between the dies and gradually pushes it inward until the desired length of material has been swaged. As the diameter is reduced the product is elongated and the operation requires only few seconds. [34]
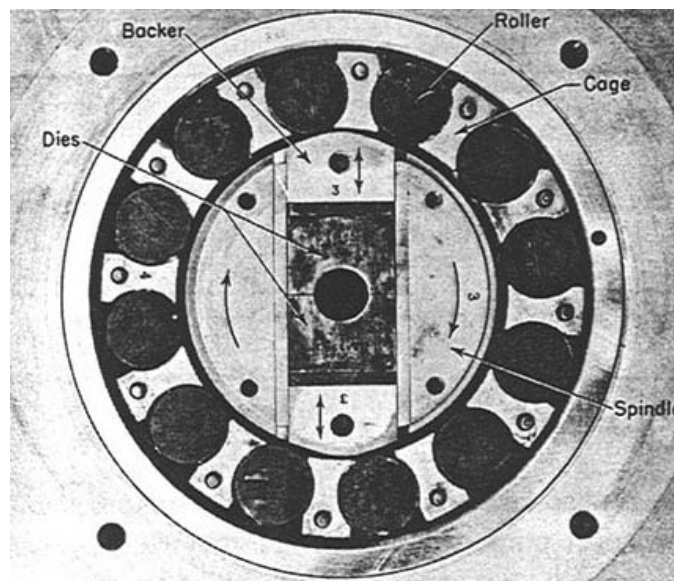

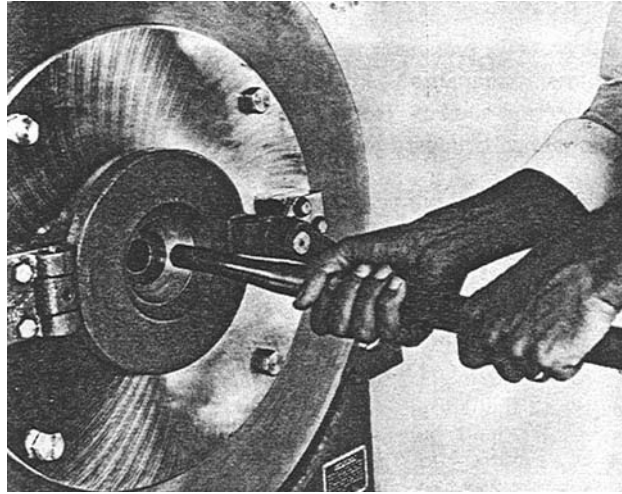Figure 2.22 Basic components and motions in a rotary swaging machine. [34]

Figure 2.23 Tube being swaged in a rotary swaging machine [34]

CHAPTER 3

EXPERIMENTAL PROCEDURE

Experimental study was carried out in order to produce three point bending specimens from AlFeVSiMg alloy powder.

3.1 Matrix Powder Production

Powder for the matrix was produced at Metallurgical and Materials Engineering Foundry Laboratory in METU. The experimental alloy was prepared by melting Al, Fe, FeV, Si and Mg in a graphite crucible. Magnesium was added after the alloy was completely melted. Induction furnace was used for this alloying. The liquid metal stream was disintegrated by air with a pressure of 15 atm. into a horizontal tank to obtain rapidly solidified powders of AlFeVSiMg alloy. The tank has dimensions of 8x2x3m to allow enough time for the powder particles to solidify before striking the walls. The set up for production of powder is in figure 3.1.
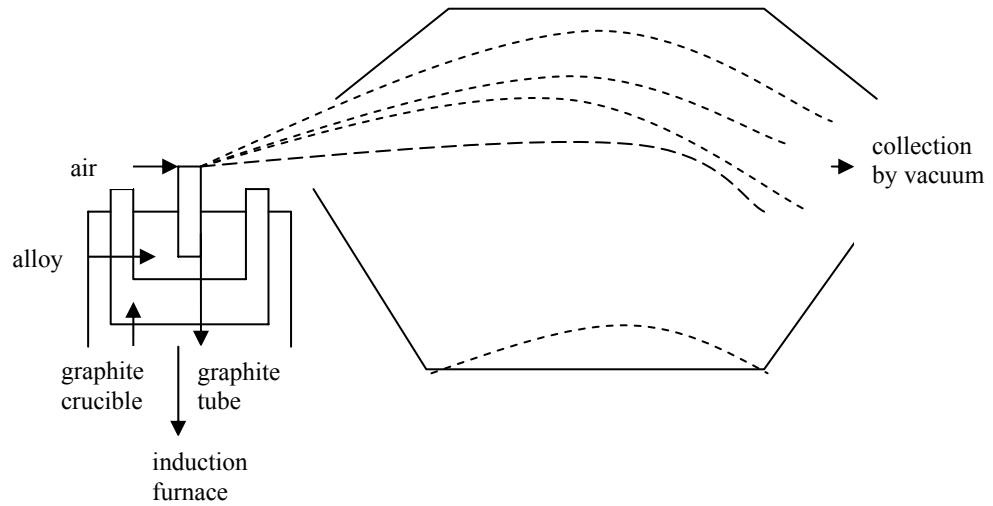
Figure 3.1. The set up for powder production

Powders were collected from the special atomization tank. The composition of powder alloy that is used for production of three point bending specimens was Al-8Fe-1.8V -8Si (in wt %) with 1%Mg treatment.

3.2 Screen Analysis

Powders with different sizes were produced during atomization. The screen analysis of the powders was in the ranges of;

-125 μm   +90 μm,

-90 μm   +63 μm,

-63 μm   +53 μm,

-53 μm   +45 μm,

-45 μm   +38 μm,

-38 μm.

3.3. Mixing

Powder lot was mixed with 1% zinc stearate which is used as solid lubricant for the preparation of all specimens except for the ones produced by single action pressing before hot dynamic compaction. Powder and zinc stearite was mixed in plastic containers with steel balls at high energy mixing condition for 30 minutes at a medium vibration.

Mixing was also done for the production of TiC reinforced specimens at the same condition explained above. TiC particles in two different amounts, 10% and 20%, were mixed with -90 μm +63 μm size powder alloy .

3.4 Canning and Cold Compaction

For all the specimens pure aluminum tubes of about 100mm length and 22mm diameter were used for canning.

Three different types of specimens were produced according to canning and cold compaction conditions.

3.4.1. Specimens That Were Produced By Using Canned Loose Powder

These specimens were produced by covering two ends of the tubes with precompacted (at 315MPa) pellets which were made from the same powder with a height of 1cm as shown in figure 3.2.
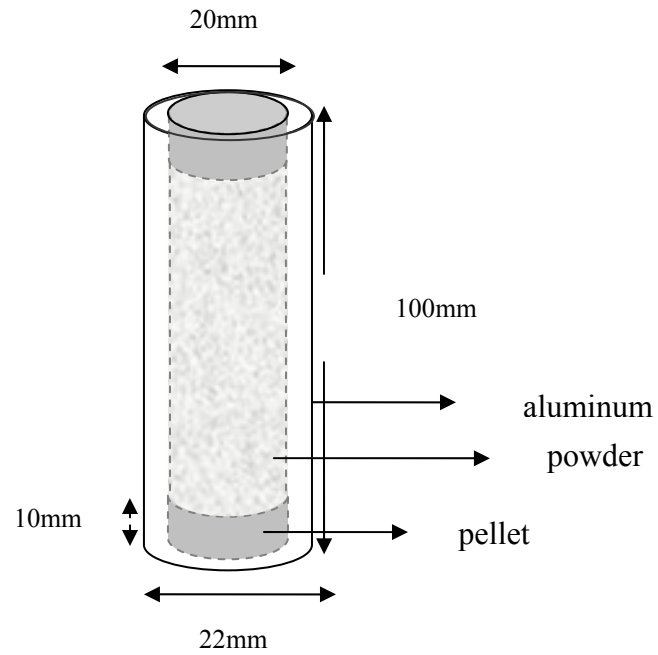
Figure 3.2. Canned loose powder

3.4.2. Specimens That Were Produced By Single Action Pressing Before Hot Dynamic Compaction

Canned powder was cold pressed with a pressure of 315 MPa by a single action press in a steel die. Figure 3.3 presents the steel mold that is used for cold compaction.
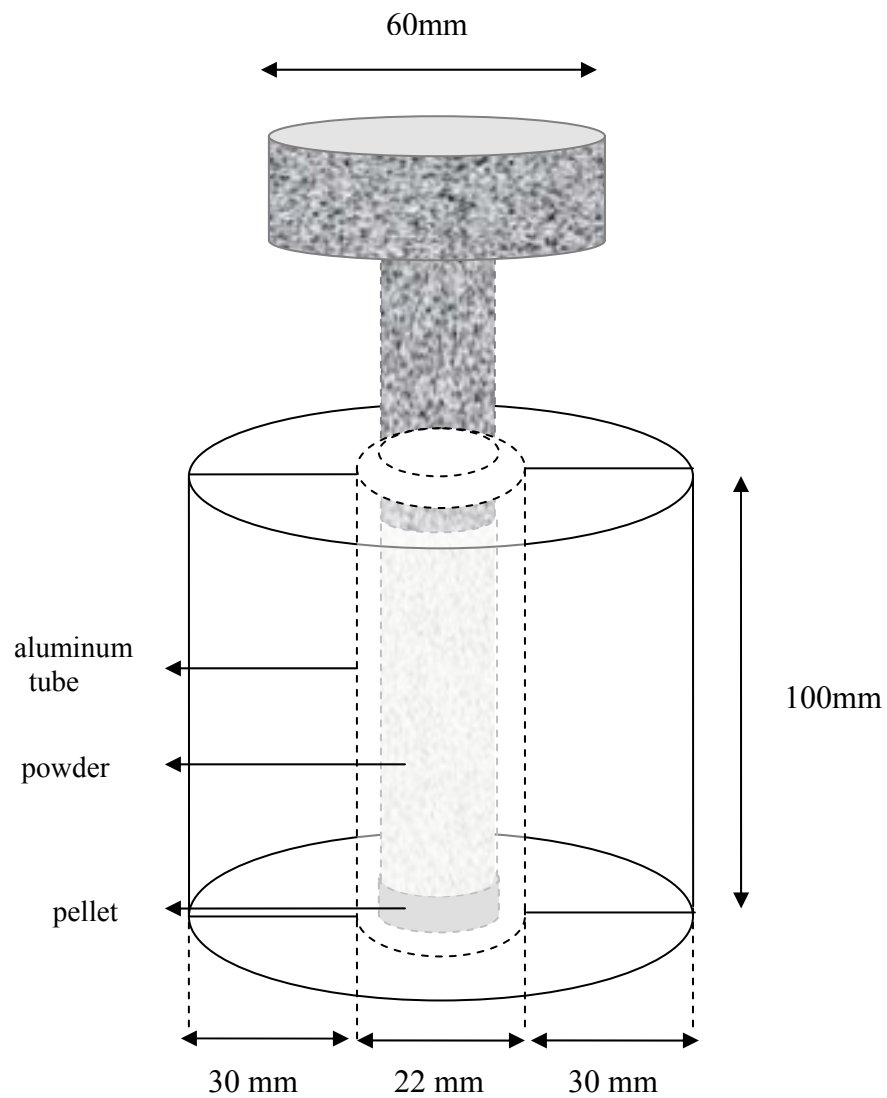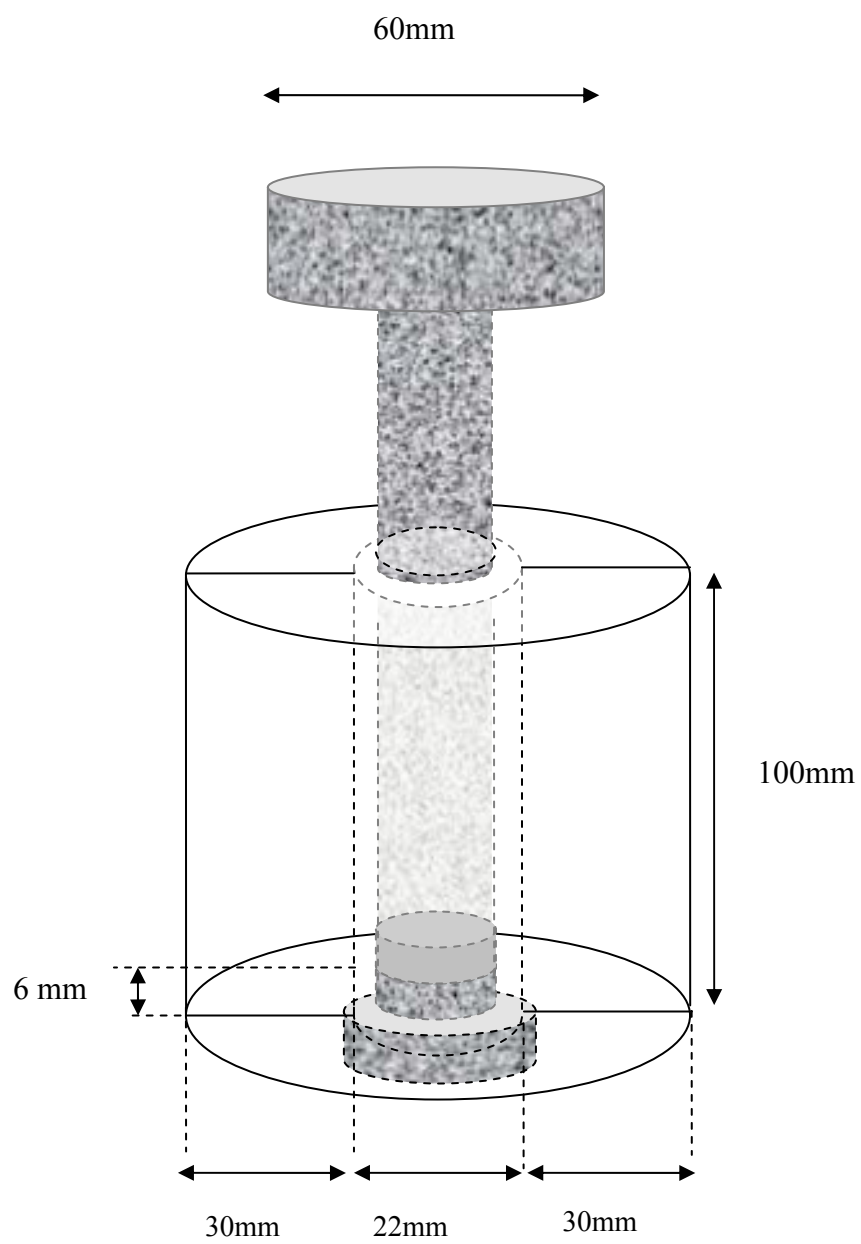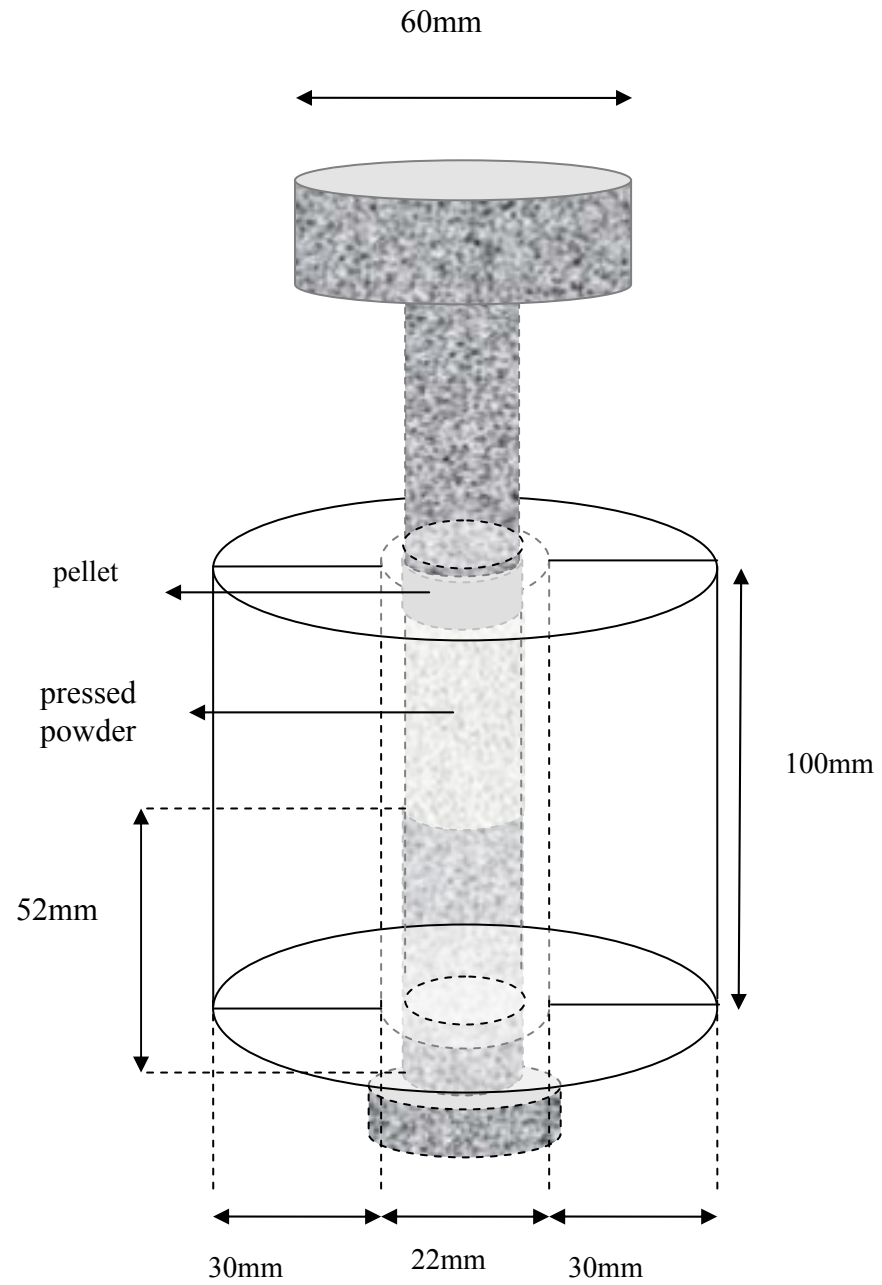
Figure 3.3. Single action pressing

3.4.3. Specimens That Were Produced By Double Action Pressing Before Hot Dynamic Compaction

For double action pressing there were two steps. First, canned powder was cold pressed with a pressure of 63 MPa in the steel die as shown in figure 3.4 (a). Then the steel die was reversed together with the canned powder and pressed again as presented in figure 3.4(b)

60mm

100mm

6 mm

30mm   22mm   30mm

(a)

43

60mm

pellet

pressed
powder

100mm

52mm

30mm

22mm

30mm

(b)

Figure 3.4. Double action pressing

3.5 Hot Dynamic Compaction

Hot dynamic compaction was done by "Swager". Swager applies pressure by the help of its rotating cylindrical die with a decreasing diameter size along its axis. The diameter of the hot compacts decreased in a two step process. After heating the compacts to 480°C for 1 hour, the canned compact swaged and a reduction in diameter from 2.2 cm to 1.97cm obtained. The compacts were reheated to 480ºC and held for 1 hour and swaged to obtain a diameter decrease from 1.97cm to 1.54cm. Drawing of swager is presented in figure 3.5. and photography of swager is shown in figure 3.6. In figure 3.7 the specimen after swaging is presented.

a) Front view   b) Side view
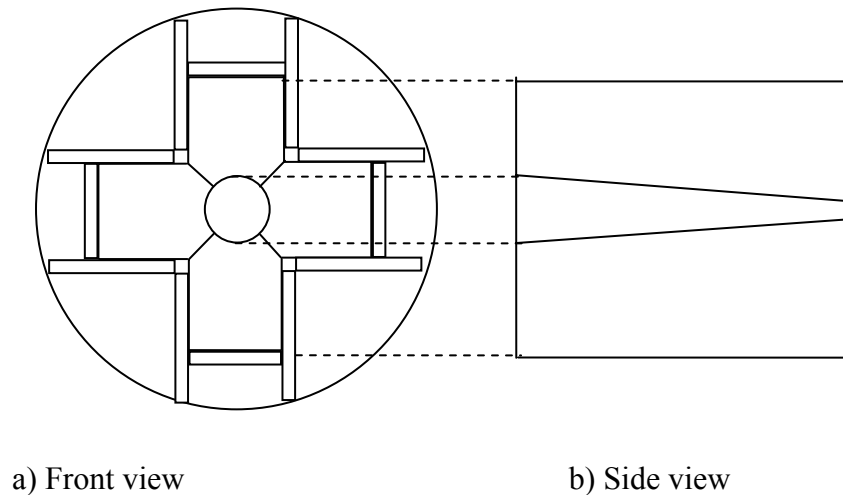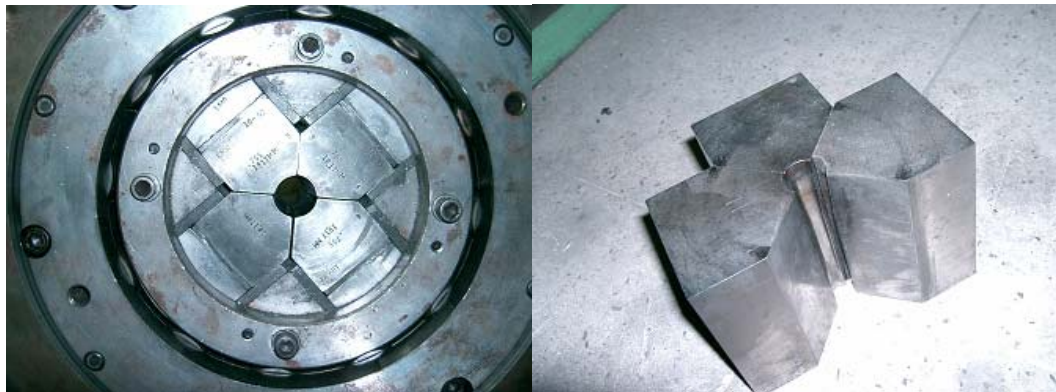
Figure 3.5. The technical drawing of the swager

a) Front view   b) Die of the swager

Figure 3.6 Photography of swager

Figure 3.7 Photography of the specimen after swaging

3.6. Three Point Bending Specimens

The compacts were machined to obtain three point bending specimens after swaging. The specimens were grinded and polished to prevent an early failure because of any surface crack. Three point bending tests were conducted at room temperature. Flexural strength of the specimens was calculated for each of the powder sizes.

Shape and dimensions of the three point bending specimens are given in figure. 3.8. Three point bending tests were done by screw driven tensile testing machine with 0.358mm/min extension rate.

span length

length = 65 mm
span length = 50 mm
b (width) = 10 mm
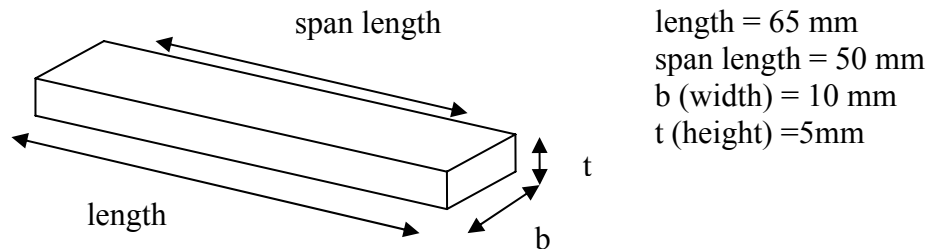t (height) =5mm

t

length

b

Figure 3.8. The geometry of three point bending specimen

Maximum loads for fracture were obtained by three point bending tests. Load in kilograms were converted to flexural stress by;

$\sigma = My/I$ where

M= Bending moment

M=P* L/4 where   P is the applied load and L is the span length of the specimen.

y= the distance from the natural axis

y= t/2 where t is the thickness of the specimen.

I= Moment of inertia

I= $b*t^3/12$ where b is the width of the specimen.

$\sigma_{max} = (3*P*L) / (2*b*t^2)$

The photography of the three point bending specinens is in figure 3.9.

Figure 3.9 Photography of the three point bending specimens

3.7 Porosity Measurement

Porosity of the specimens was measured by Archimedes Principle with xylene.

3.8 Differential Scanning Calorimetry (DSC) Analysis

Differential Scanning Calorimetry (DSC) analysis was done in Central Laboratory of METU.

3.9 Heat Treatment

A heat treatment was applied to specimens at 190°C for 1, 2, 3, 4, 6 and 8 hours in order to determine the formation of Mg_2Si.

3.10 X-Ray Study

X-Ray study was carried out in order to identify the phases in specimens. The study was performed by a Philips PW-1352/20 twin tube diffraction unit operating at

35KV tube voltage. CoKα radiation with a wavelength of 1.79Å was used. The energy level was 30KV.

3.11 SEM Study

Scanning Electron Microscopy study was carried out by using JSM-6400 Electron Microscope JEOL., equipped with NORAN system. Specimens were etched by Keller's etchant.

3.12 Hardness Test

Hardness tests were done by Heckert Analogue Hardness Testing Machine.

CHAPTER 4

RESULTS AND DISCUSSION

The effect of hot dynamic consolidation on the mechanical properties of air atomized AlFeVSi alloy has been evaluated in this study. The initial alloy composition was Al-8Fe-1.8V-8Si with 1% Mg (wt%) and EDS analysis of the alloy is given in table 4.1 below.

The relation between powder size and mechanical properties were investigated. The production of three point bending specimens varied according to pressing conditions before hot dynamic compaction, as explained at Chapter 3. The change in production method affected the results of mechanical tests.

Production of particulate reinforced composites and effect of reinforcement amount to the mechanical behavior of the composites are also in the scope of this study. A set of specimens reinforced with TiC particulates had been prepared. Some of the reinforced specimens were produced by double action pressing and some of them were only canned before hot dynamic compaction. The alloy compositions of both unreinforced and reinfoced alloy were the same.

Table 4.1 EDS analysis of the cast alloy

	Al	Fe	V	Si	Mg
Weight Conc%	79.42	9.81	1.19	9.25	0.35
Atom Conc%	84.44	5.04	0.67	9.44	0.41

4.1 Results of Three Point Bending Test

The first set of specimens was produced by single action pressing before hot dynamic compaction. The results of three point bending specimens are given in table 4.2.

Table 4.2.The results of three point bending tests of specimens produced by single action pressing before hot dynamic compaction.

Matrix powder size	Maximum flexural strength (MPa)	Precompaction pressure (MPa)	Comments
+90 μm	313	315 *	Sound specimens were obtaiened
+63 μm	316	315 *	Sound specimens were obtaiened
+53 μm	259	315 *	Sound specimens were obtaiened
+45 μm	-	315 *	Surfacecrack was observed
+38 μm	-	315 *	Broken during machining
-38 μm	-	315 *	Broken during machining

(*No lubricant added)

Although some of the specimens have reasonable maximum flexural stresses, some specimens fractured at very low stress values. The reason of these low values may be attributed to the delamination(transverse) cracks on the surface of the specimens as shown in figure 4.1.

Figure 4.1 Photography of the specimen with a delamination crack

To avoid delamination cracks, double action pressing before swaging and addition of 1% zinc stearate as solid lubricant were applied. The results of three point bending tests of specimens produced by double action pressing before swaging are presented in table 4.3.

Table 4.3. The results of three point bending tests of the specimens produced by double action pressing before swaging

Matrix powder size	Maximum flexural strength (MPa)	Precompaction pressure (MPa)	Comments 1% Zinc stearate lubricant addition
+90 μm	233	63	Sound specimens
+63 μm	152	63	Sound specimens
+53 μm	72	63	Sound specimens
+45 μm	239	63	Sound specimens
+38 μm	-	63	Broken during machining

Some specimens were produced without applying pressing process before hot swaging. The results of three point bending tests of these specimens are given in the table 4.4. below.

Table 4.4. The results of three point bending tests of specimens produced without applying pressing process before swaging.

Matrix powder size	Maximum flexural strength (MPa)	Precompaction Pressure (MPa)	Comments 1% Zinc stearate lubricant addition
+90 μm	135	0	Sound specimens
+63 μm	76	0	Sound specimens
+53 μm	147	0	Sound specimens
+45 μm	177	0	Sound specimens
+38 μm	189	0	Sound specimens

Although the results of the three point bending tests showed that specimens produced by double action pressing had higer maximum flexural strength values than the ones produced by canning of loose powders, there were delamination cracks at these double pressed specimens. No delamination cracks were observed at specimens produced by canning of loose powders.

Two different sets of specimens, double action pressed and canned loose powders, were prepared for the production of TiC reinforced MMC specimens. The results of three point bending tests of these specimens are given in the table 4.5. below.

Table 4.5. The results of three point bending tests of the specimens reinforced with TiC particulates

	Matrix powder size	TiC %	Precompaction Pressure(MPa)*	Maximum flexural strength (MPa)
Double action pressing before swaging	+63 µm	10	63	285
No pressing(canned loose powders)	+63 µm	10	0	190
Double action pressing before swaging	+63 µm	20	63	189
No pressing	+63 µm	20	0	87

(*1% Zinc stearate lubricant addition)

As it is seen from the table, significant increase in maximum flexural stess had been obtained in the 10% TiC reinforced samples that were produced by double action pressing before hot dynamic compaction. Also, maximum flexural stress of 10% TiC reinforced specimens had better results than 20% TiC reinforced specimens.

In figure 4.2, the graph of maximum flexural strength vs powder size for all type of specimens is given.
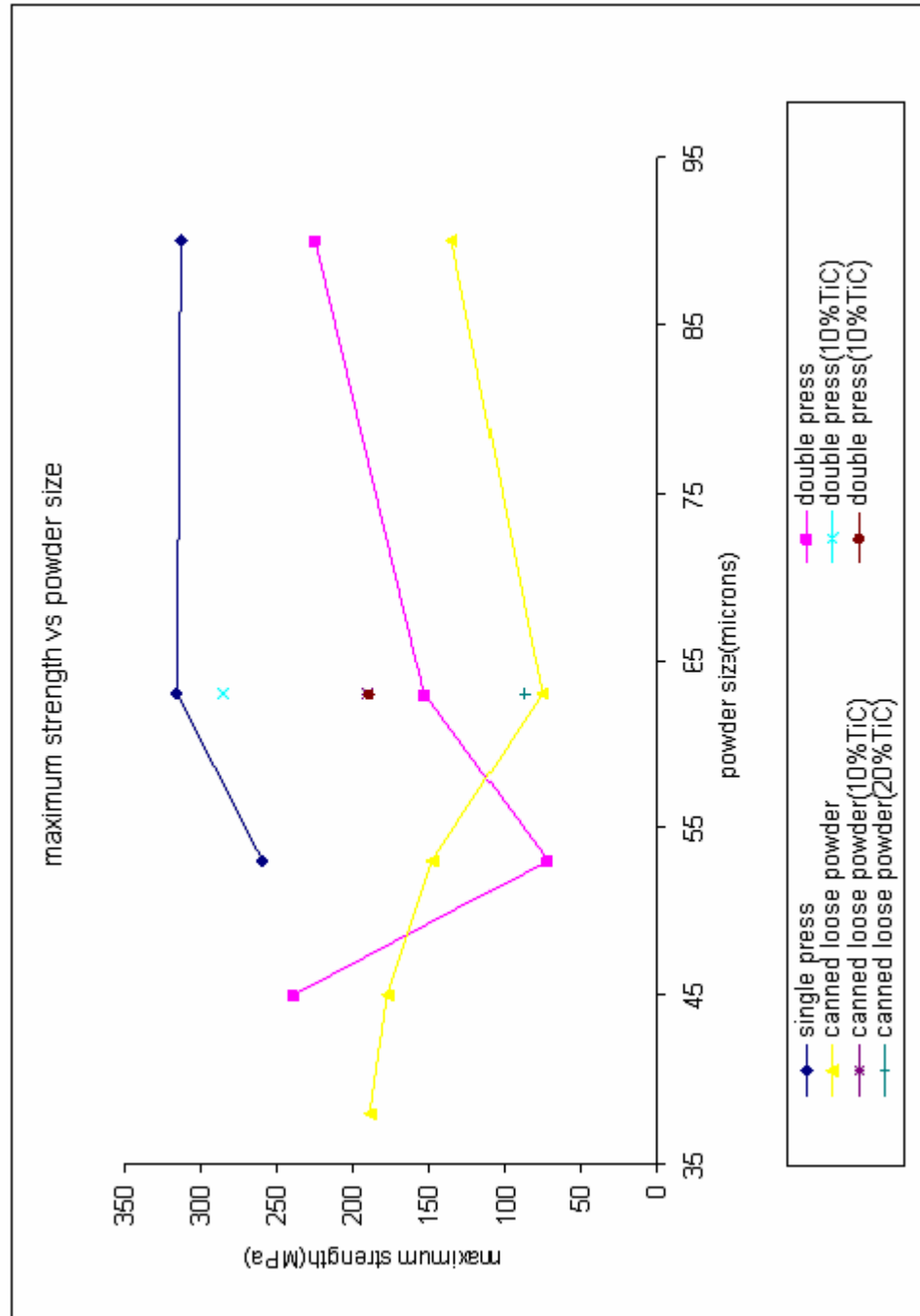
maximum strength vs powder size

Figure 4.2 Maximum flexural strength vs. powder size

54

In table 4.6, elastic modulus values of some of the specimens are given.

T able 4.6, elastic modulus of some of the specimens

Specimen powder size	Process	TiC%	Precompaction Pressure(MPa)*	Elastic Modulus(GPa)
+90 μm	DP	0	63	40
+90 μm	LP	0	0	33
+63 μm	DP	10	63	51
+63 μm	DP	20	63	30
+63 μm	LP	10	0	31
+63 μm	LP	20	0	51
+53 μm	DP	0	63	30
+53 μm	LP	0	0	32
+45 μm	DP	0	63	27
+38 μm	LP	0	0	31

(*1% Zinc stearate lubricant addition, DP double press, LP loose powder befere swaging)

4.2 Results of Hardness Tests

Hardness of the three point bending specimens that were produced by single action pressing before swaging were given in table 4.7 and figure 4.3. Maximum hardness values were obtained for the specimens which were produced with the smallest powder size and minimum hardness values were obtained for specimens which were produced with the highest powder size. There was not significant difference in hardness values of +53μm and +63μm powder size specimens.

Table 4.7 Hardness of the specimens produced by single action pressing

Specimen powder size	Hardness(BHN)				
	1	2	3	4	Avarage
+90 μm	105	112	109	102	107
+63 μm	121	116	116	112	116
+53 μm	121	112	112	112	114
+45 μm	135	130	125	125	129
+38 μm	130	125	135	121	128
-38 μm	151	145	145	145	147
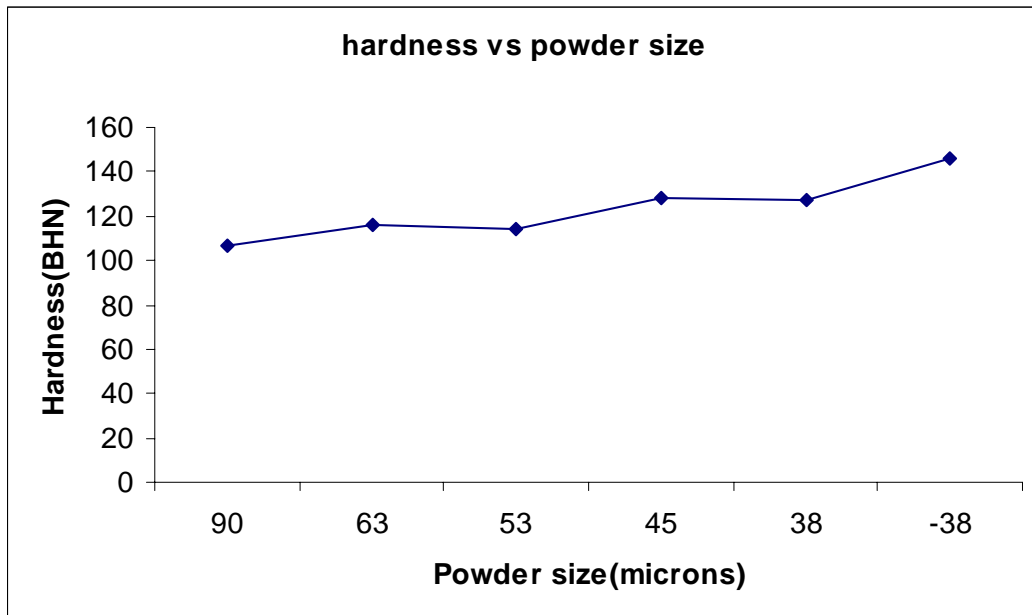
Figure 4.3 Graph of hardness vs. powder size for the specimens produced by single pressing

Artificial aging was applied to the specimen by holding at 190ºC for 1, 2, 3, 4, 6 and 8 hours. The result of this heat treatment is given in figure 4.4. Formation of Mg_2Si was investigated but the existence of this phase could not be proved by X-ray and SEM study.
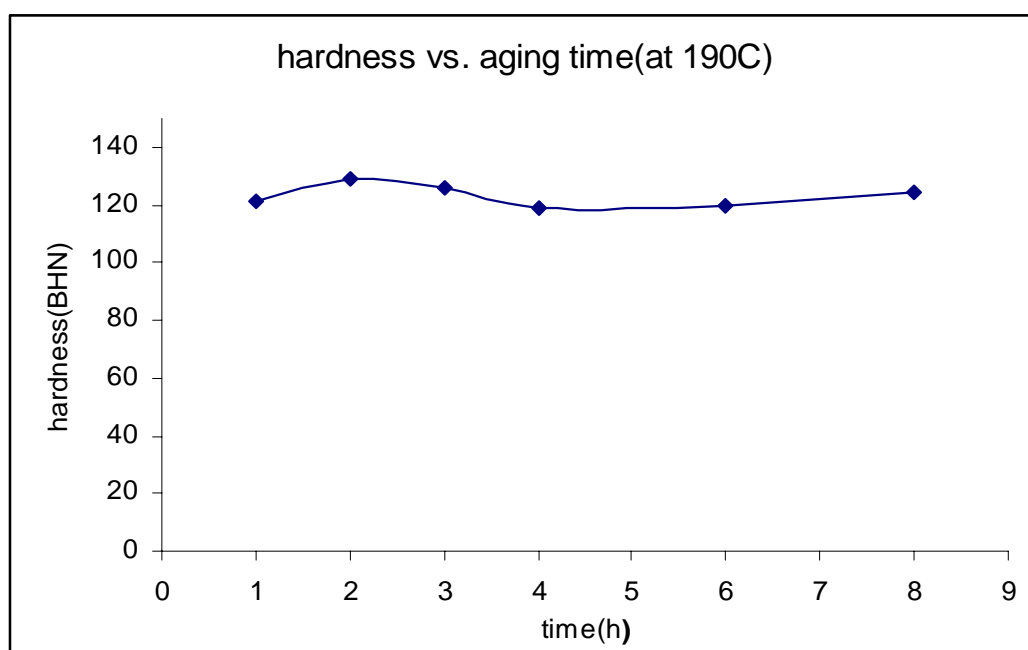

Figure 4.4. The result of artificial aging at 190°C

From figure 4.5 to 4.10 comparison for hardness of specimens produced by double action pressing and canning of loose powder before swaging is presented. As it is seen from these figures; generally, double action compaction had increased the hardness values of specimens.
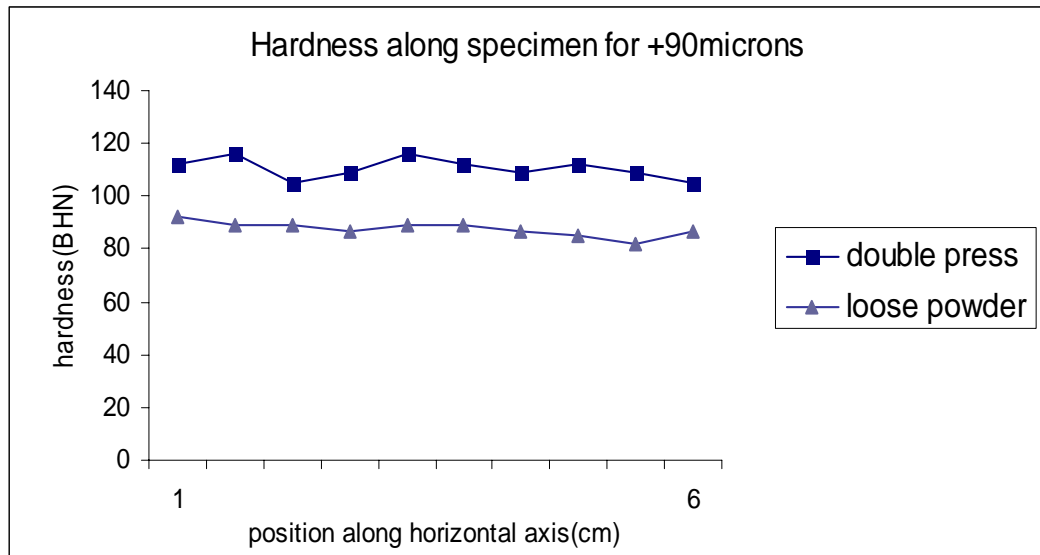
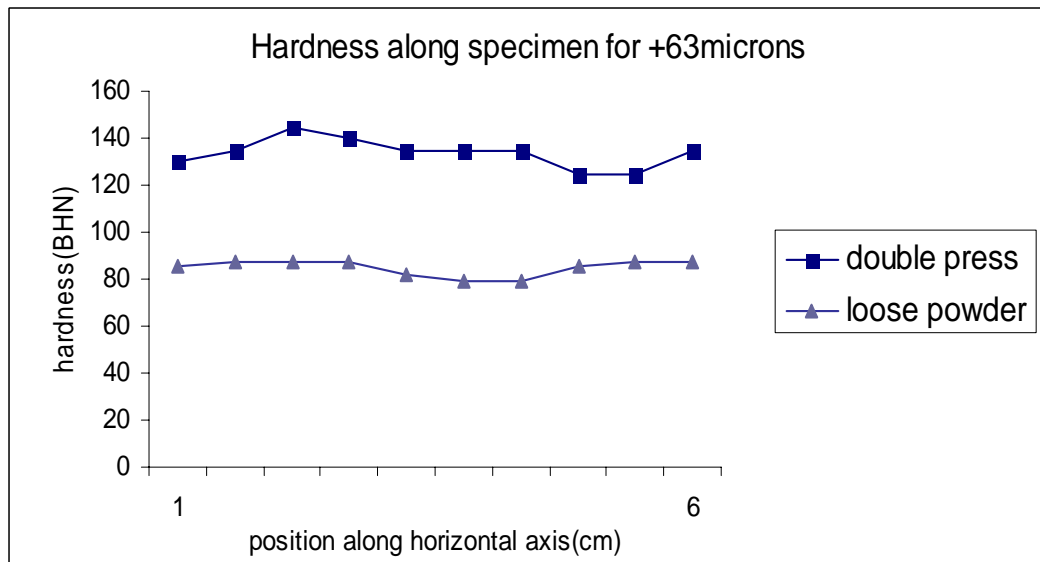Figure 4.5. Hardness along specimens which were produced from +90μm alloy powder

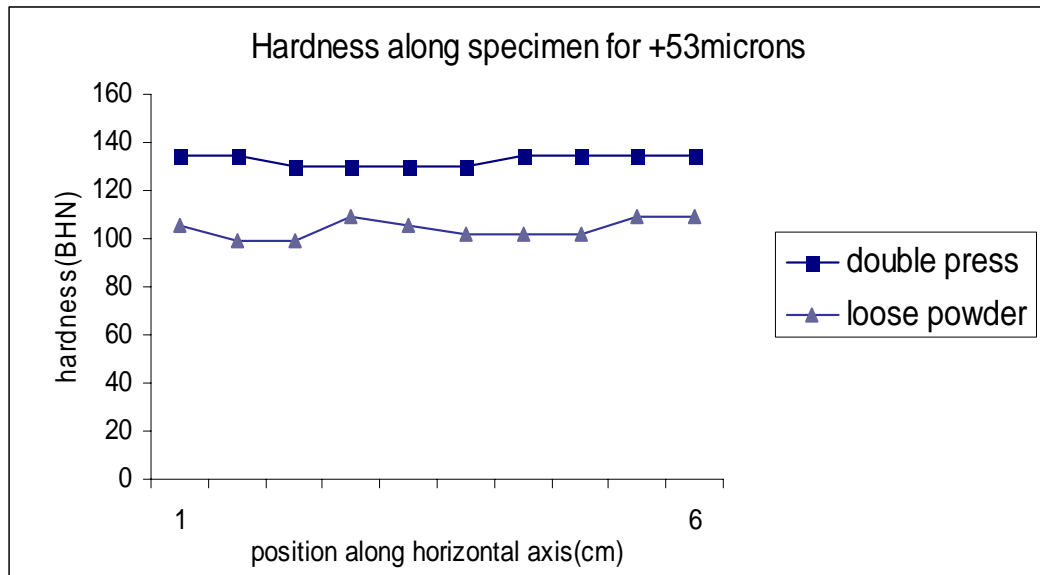Figure 4.6. Hardness along specimens which were produced from +63μm alloy powder

Figure 4.7. Hardness along specimen which were produced from +53μm alloy powder

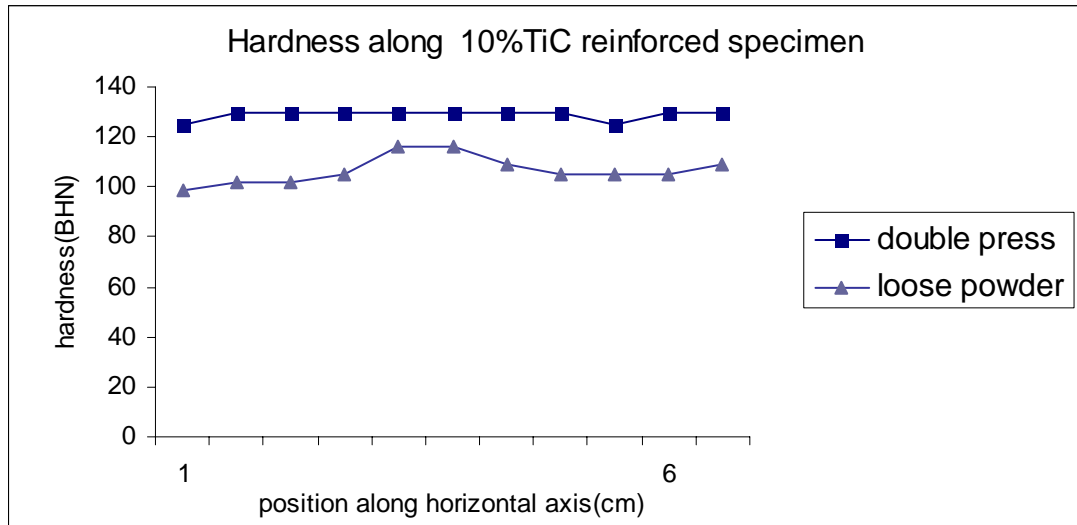Figure 4.8. Hardness along specimen which were produced from +45 μm alloy powder

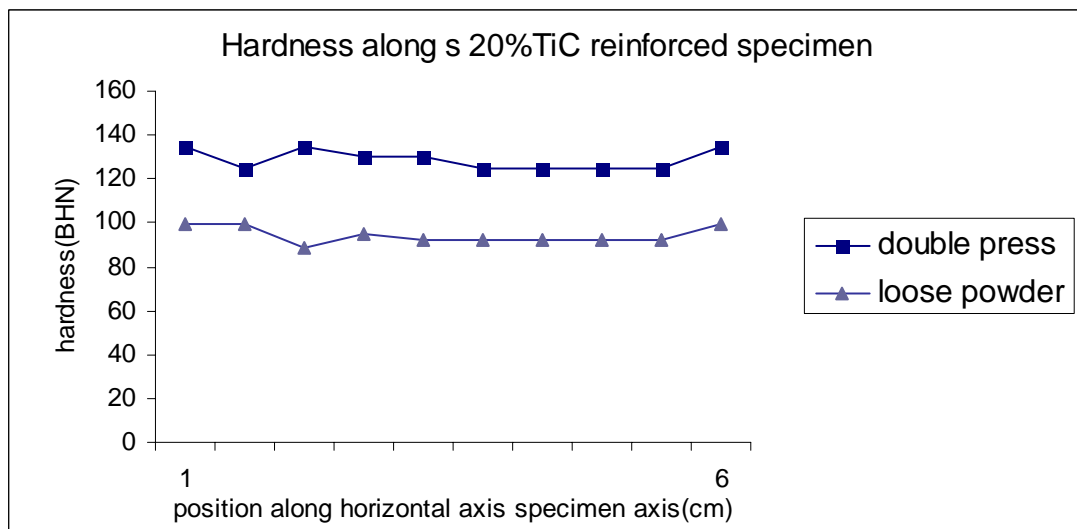Figure 4.9. Hardness along specimens which were produced from 10% TiC reinforced +63μm alloy powder

Figure 4.10. Hardness along specimen which were produced from 20% TiC reinforced +63μm alloy powder

The hardness values of all specimens and a comparison of hardness values are given in table 4.8 and figure 4.11.

Table 4.8 Hardness values of all the specimens produced

Specimen powder size	Process	TiC %	Hardness (BHN)										Avarage
			1	2	3	4	5	6	7	8	9	10	
+90 μm	DP	0	112	116	105	109	116	112	109	112	109	105	110.5
+90 μm	LP	0	92	89	89	87	89	89	87	85	82	87	87.6
+90 μm	SP	0	105	112	109	102							107
+63 μm	DP	0	130	135	145	140	135	135	135	125	125	135	134
+63 μm	LP	0	85	87	87	87	82	79	79	85	87	87	84.5
+63 μm	SP	0	121	116	116	112							116
+63 μm	DP	10	125	130	130	130	130	130	130	125	130	130	129
+63 μm	LP	10	99	102	102	105	116	116	109	105	105	109	106
+63 μm	DP	20	135	125	135	130	130	125	125	125	125	135	129
+63 μm	LP	20	99	99	89	95	92	92	92	92	92	99	94
+53 μm	DP	0	135	135	130	130	130	130	135	135	135	135	133
+53 μm	LP	0	105	99	99	109	105	102	102	102	109	109	104.1
+53 μm	SP	0	121	112	112	112							114
+45 μm	DP	0	135	145	145	145	145	145	145	145	140	140	143
+45 μm	LP	0	112	109	112	116	109	116	105	109	112	109	110,9
+45 μm	SP	0	135	130	125	125							129

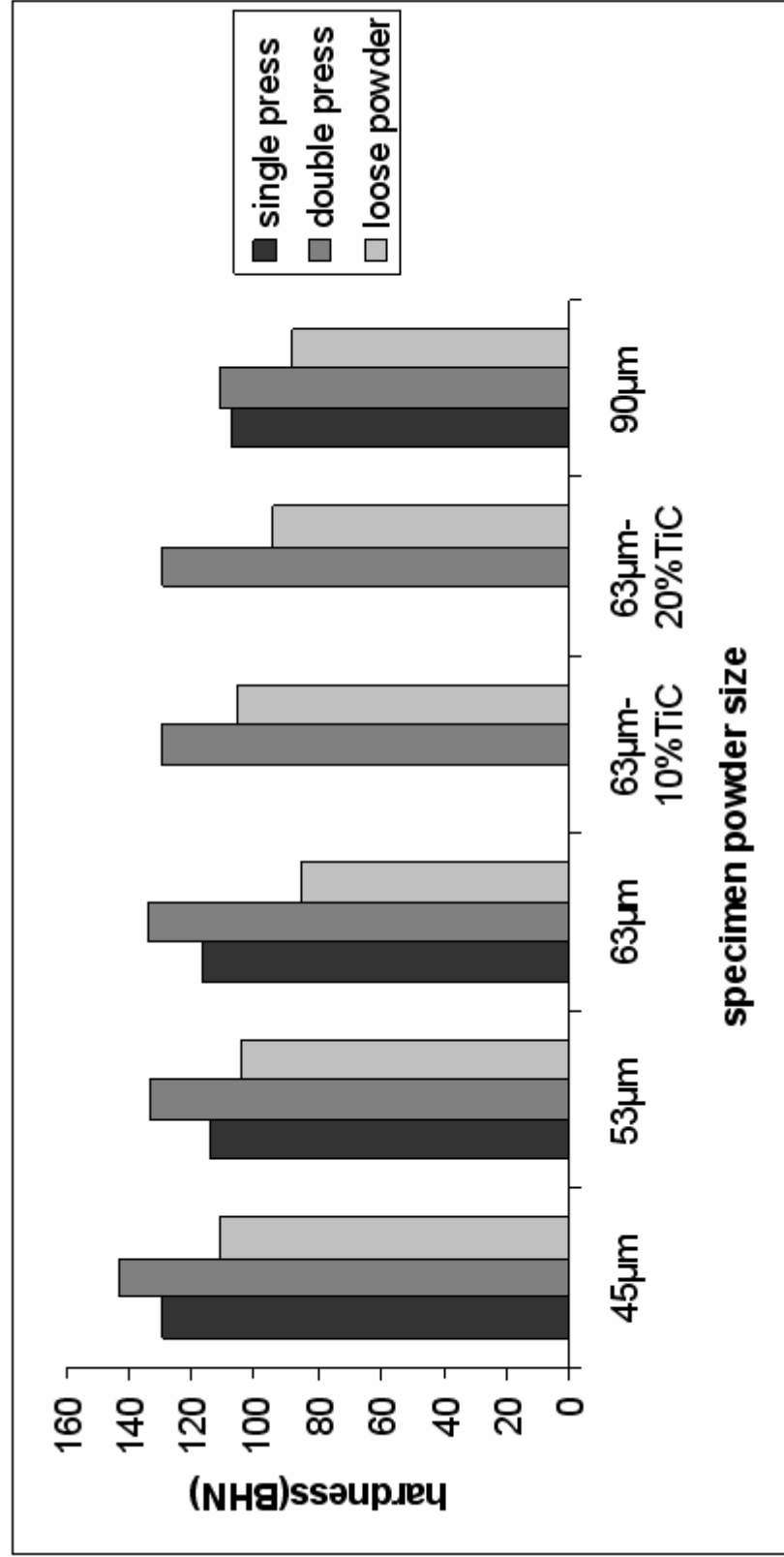(DP double action pressing, LP canning of loose powder, SP single action pressing)

Figure 4.11 Comparison of specimen powder size, processing method and avarage hardness values

As it is seen from figure 4.11, there was an increase in hardness of specimens when the processing method was changed from cannning of loose powders to single action pressing. The highest hardness values were obtained for double action pressed specimens.

4.3 Results of X-Ray Study

By X-ray analysis, the formation of Mg_2Si was investigated. X-ray patterns of the specimens that were artificially aged at 190°C for different hours are shown in figure 4.12. As it is seen from the figure there was no significant change in patterns.
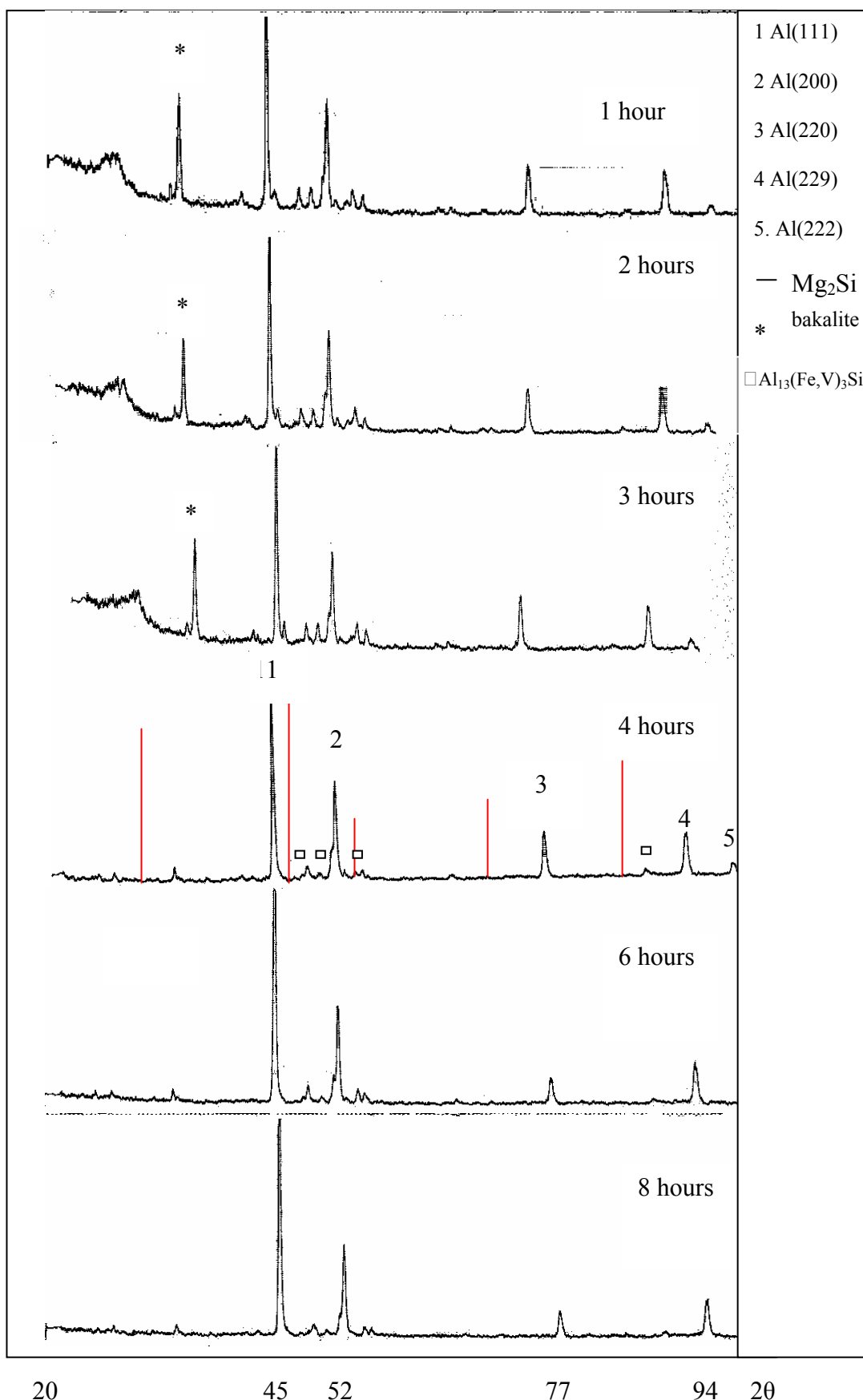
Figure 4.12.XRD patterns of specimens after heat treatment at 190°C

I

1 Al(111)

2 Al(200)

3 Al(220)

4 Al(229)

5. Al(222)

— Mg₂Si

* bakalite

□ Al₁₃(Fe,V)₃Si

1 hour

2 hours

3 hours

4 hours

6 hours

8 hours

20   45   52   77   94   2θ

The XRD pattern of the specimen produced from alloy powder of size -90μm +63μm and the XRD pattern of the alloy powder are shown in figure 4.13. As it is seen from the figure solid phase crystal structure was stable after processing.
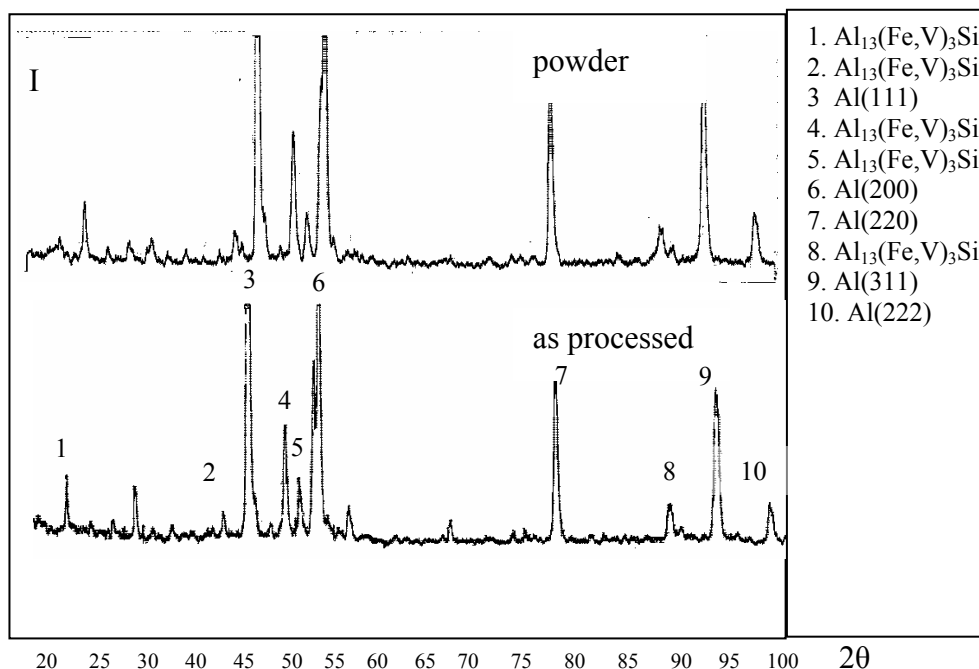

Figure 4.13.XRD pattern of the alloy powder of +63μm size and XRD pattern of the specimen produced from the same powder

The XRD pattern of the specimen produced from alloy powder of size +53μm is shown in Figure 4.14. X-ray analysis was done to determine the phase that was observed in SEM micrograph of the part of the specimen which was vertical to the swaging direction. The phase was possibly $Al_{0.7}Fe_3Si_{0.3}$.
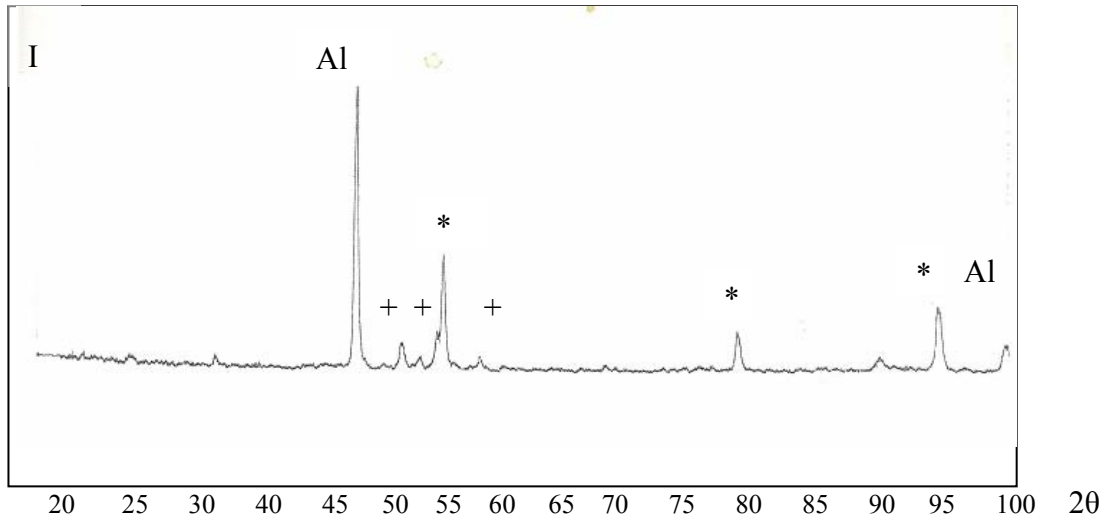
65

Figure 4.14 The diffractogramme of the part of specimen vertical to the swaging direction produced with alloy powder of size +53μm.

(* Al $_{0.7}$Fe$_3$Si$_{0.3}$, + Al$_{13}$(Fe,V)$_3$Si)

4.4 Results of Porosity Measurement

Porosity of the specimens were calculated by comparing the densities of the three point bending specimens with the density of the cast specimen of the same alloy. The results of porosity measurement is presented in table 4.9.

Table 4.9. The results of porosity measurement of the specimens

Process	SP	DP	LP
Specimen powder size	Porosity %	Porosity %	Porosity %
+90 μm	1.10	~0	7.00
+63 μm	0.03	~0	6.00
+53 μm	1.10	~0	3.00
+45 μm	~0	~0	10.00
+38 μm	0.08	~0	3.00
-38 μm	0.39		

(SP single press, DP double press, LP loose powder befere swaging)

66

In double pressed specimens, there were no considerable porosity. High porosity of the specimen of -38 µm powder size may be attributed to the high interparticle friction due to the small initial powder size.

4.5. Results of DSC

The results of DSC analysis which were obtained at a rate of 20°C/min. are presented in figures 4.15-4.19. The peaks seen in figures are endothermic reactions that show Ts of the alloy.
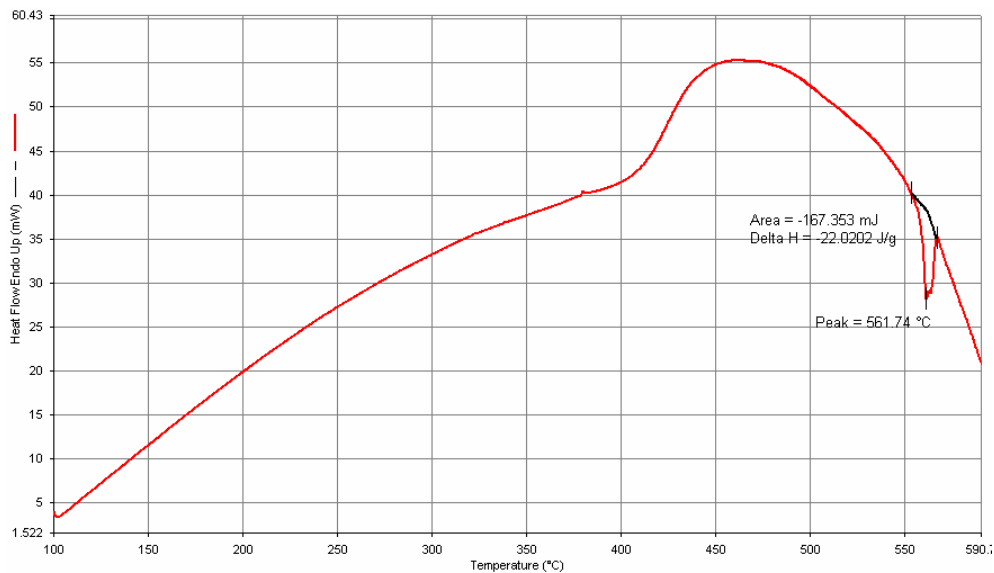

Figure 4.15 DSC analysis of the specimen with a powder size of +53 microns.
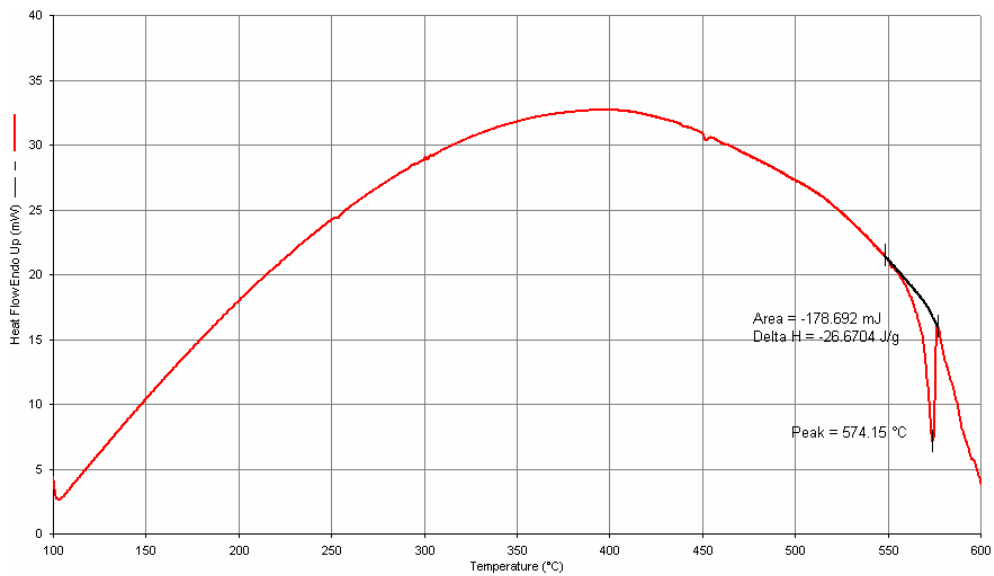
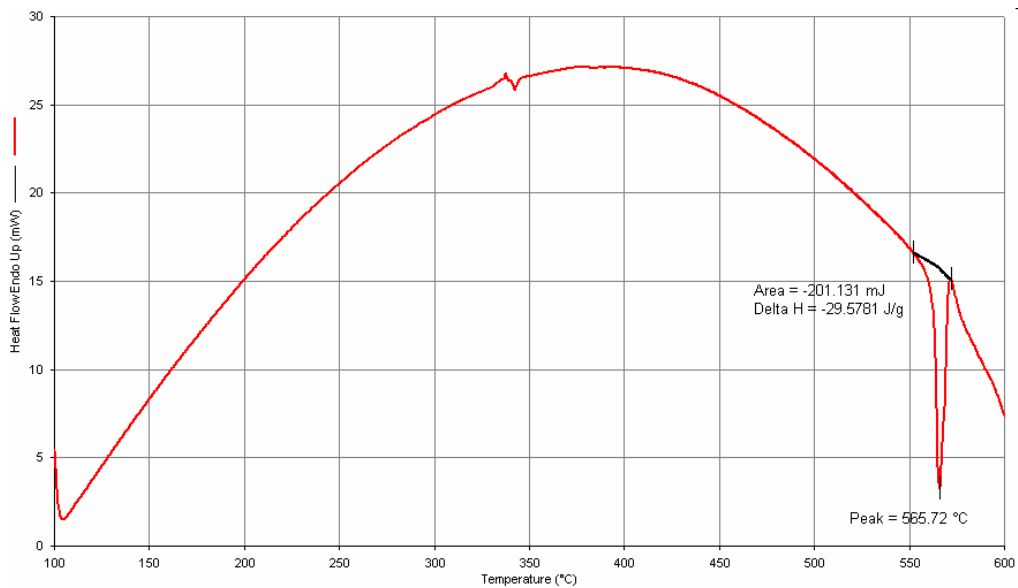Figure 4.16 DSC analysis of the specimen with a powder size of -38 microns.

Figure 4.17.DSC analysis of the specimen with a powder size of +90 microns.
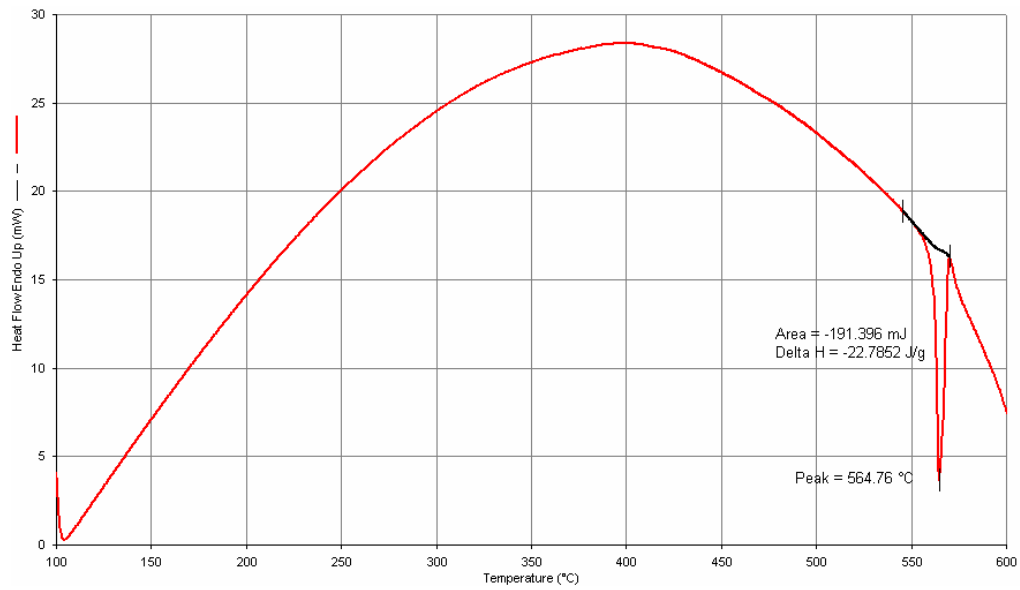
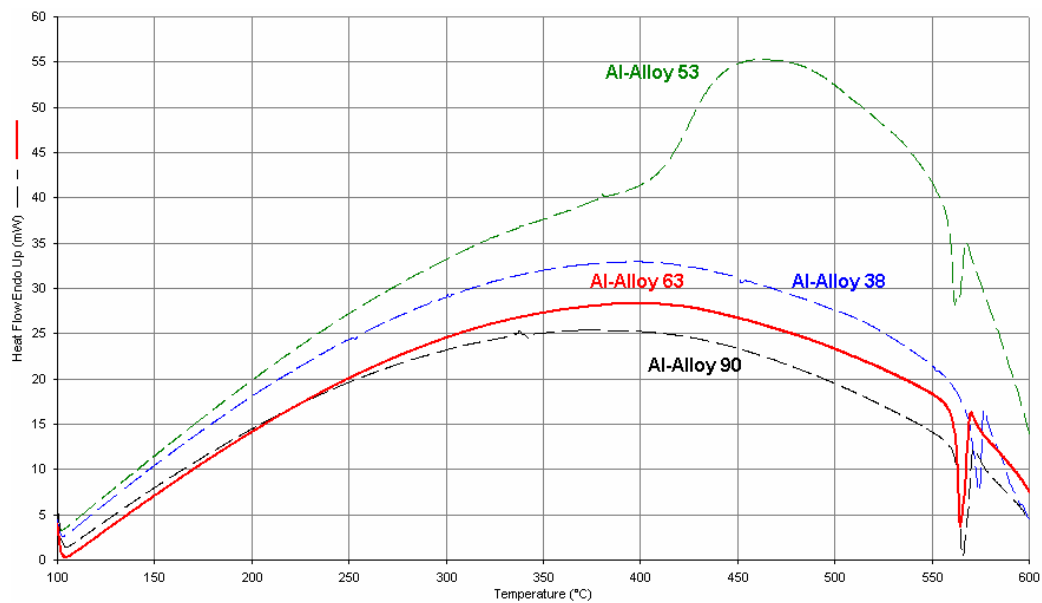Figure 4.18 DSC analysis of the specimen with a powder size of +63 microns.

Figure 4.19 DSC analysis of all results for comparison

As it is seen from above figures, no significant phase tranformation peak was detected on the curves confirming the microstructural stability up to the melting temperature.

69

4.6. Results of SEM Study

SEM micrographs were taken from the part of the specimens parallel to the swaging direction.

In figure 4.20 SEM micrograph of specimens produced from powders that are smaller than 38 μm is presented. There were some star shape particles in a few grains. EDS analysis of the specimen matrix and star like precipitate is in table 4.10.
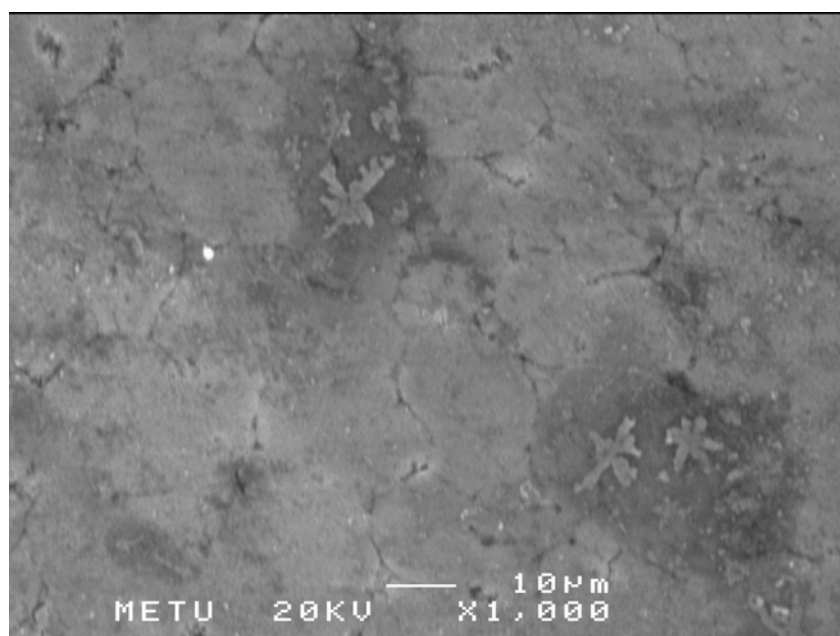

Figure. 4.20 SEM micrograph of specimen produced from -38 micron alloy powder by single action pressing before swaging

Table 4.10. EDS analysis of the specimen produced from powders of -38μm

Location	Composition in wt%			
	Al	Si	V	Fe
star like precipitate	80.40	9.61	1.40	8.58
matrix	82.99	8.43	1.79	6.79

In figure 4.21, Backscattered SEM micrograph of specimen produced with powder of +38 micron by single action pressing consists of three main regions. Silicides indicated by number 1 has a composition of Al-9.82Si-16.88Fe-4.33V with near spherical shape. The size of silicides showed a variation. The maximum value was about 3 microns. Silicide rich matrix regions indicated by number 2 had a composition of Al-34.82Si-0.85V-1.47Fe, while silicide free region indicated by number 3 had a composition of Al-6.52Si-1.69V-7.19Fe.
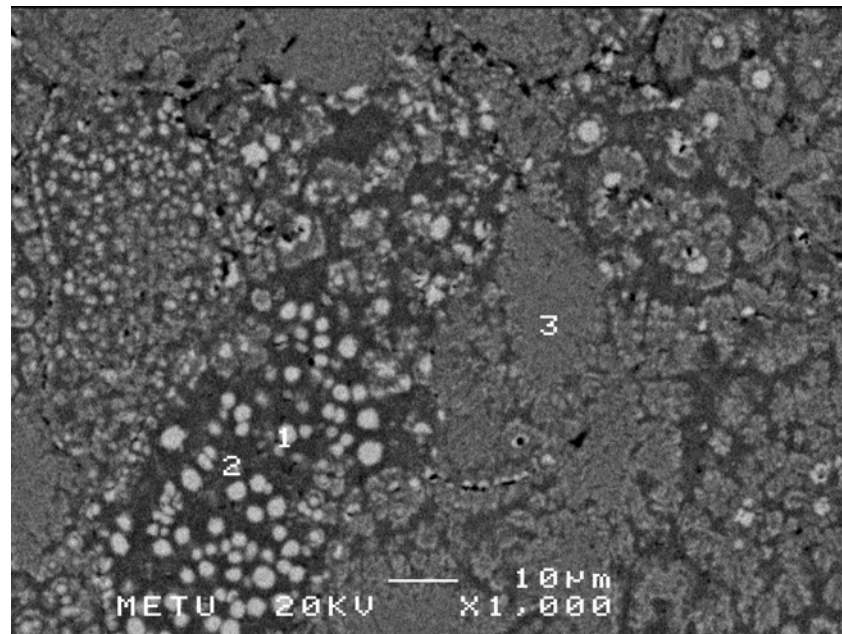

Figure 4.21 Backscattered SEM micrograph of specimen produced from +38 micron alloy powder by single action pressing before swaging

Table 4.11. EDS analysis of the specimen produced from powders of +38μm

Location	Composition in wt%				
	Al	Si	V	Fe	Mg
silicide(1)	68.98	9.82	4.33	16.88	
matrix (2)	62.42	34.82	0.85	1.47	0.49
matrix (3)	84.54	6.52	1.69	7.19	0.05

71

In figure 4.22, Backscattered SEM micrograph of specimen produced from +45 micron alloy powder by single action pressing before swaging. Grains and pores between grains can be seen.
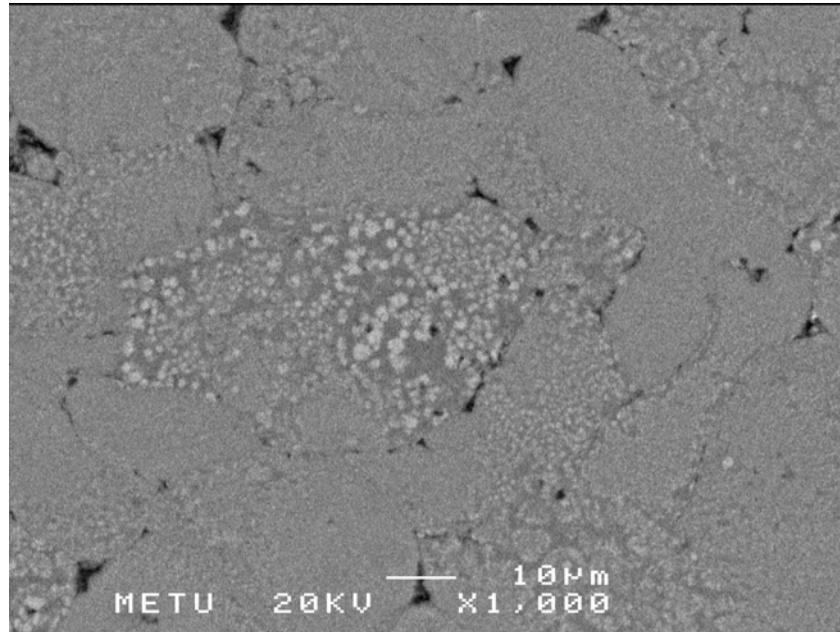

Fig. 4.22 Backscattered SEM Micrograph of specimen produced with powder size of +45 micron.

Figure 4.23 and 4.24 shows SEM micrograph of the specimen produced with +53 micron alloy powder by single pressing before swaging. Micrograph was taken from the cross section of the specimen vertical to the swaging direction. Composition of the vanadium free phase indicated by number 1 is Al-17.29Si-8.34Fe. This phase existed in the outer regions of the specimen. Matrix of the specimen around this vanadium free phase had a composition of Al-7.12Si-1.43V-8.69Fe.
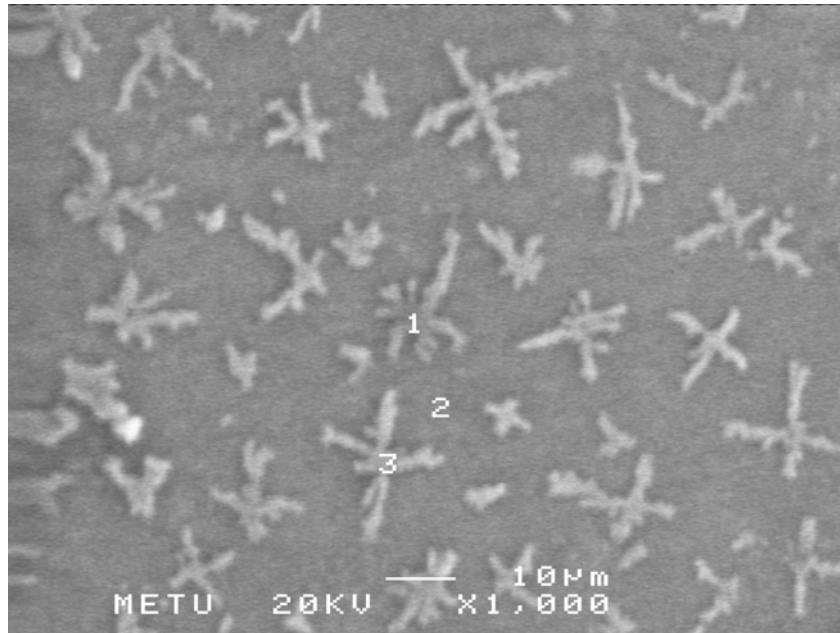
Figure 4.23 SEM Micrograph of specimen produced from powder with a size of +53 micron(vertical to the swaging direction)
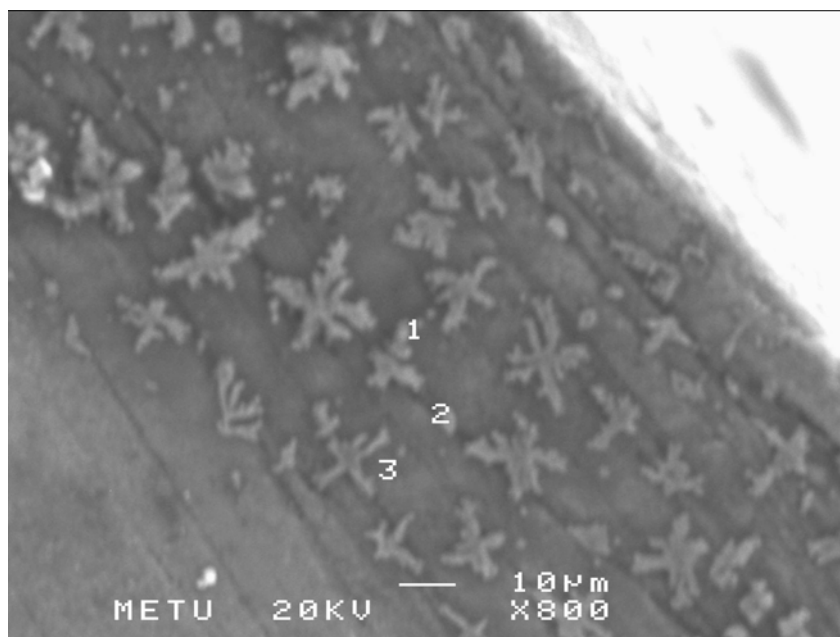

Fig. 4.24 SEM Micrograph of specimen produced from powder with a size of +53 micron(vertical to the swaging direction)

Table 4.12. EDS analysis of the specimen produced from powders of +53μm

Location	Composition in wt%				
	Al	Si	V	Fe	Mg
star like precipitate(1)	74.37	17.29		8.34	
matrix (2)	82.77	7.12	1.43	8.69	
matrix (3)	80.06	67.27	2.44	71.23	

Figure 4.25 shows backscattered SEM micrograph of the specimen produced from powder with a size of +53 micron by single action pressing.

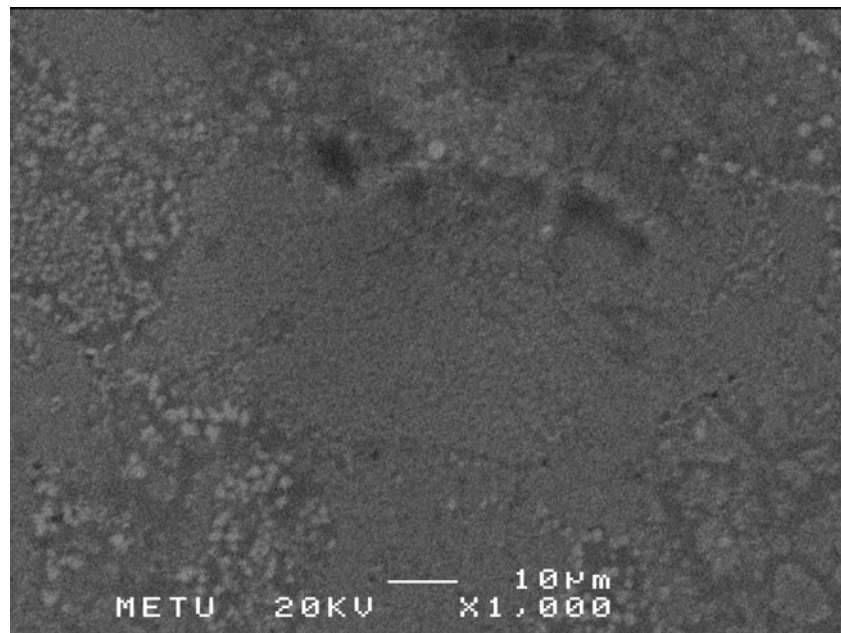Figure 4.25 Backscattered SEM micrograph of the specimen produced with powder size of +53 μm

Table 4.13. EDS analysis of the specimen produced from powders of +53μm

Location	Composition in wt%				
	Al	Si	V	Fe	Mg
silicide	71.34	23.32	1.34	3.99	

In figure 4.26, Backscattered SEM micrograph of specimen produced with powder size of +63 micron, three regions were shown. Region 1 indicates silicides with a composition of Al-8.34Si-3.7V-16.44Fe. There were two types of matrices. The composition of darker areas indicated by 2 was Al-13.88Si-1.03V-4.85Fe and composition of lighter areas indicated by 3 was Al-4.33Si-1.96V-7.57Fe. Another analysis of light matrix area gave a result of Al-3.57Si-1.81V.8.58Fe.
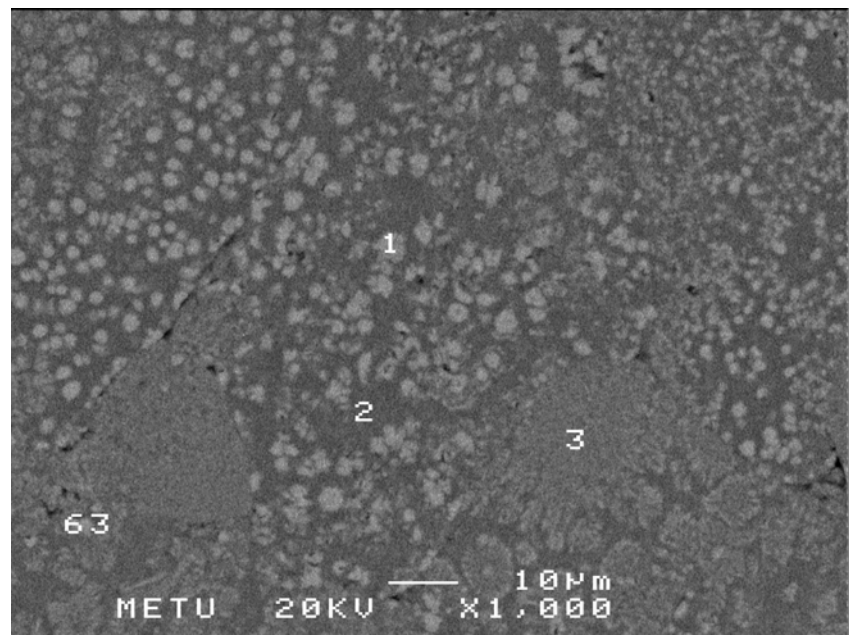

Fig. 4.26. Backscattered SEM micrograph of specimen produced with powder size of +63 micron by single action pressing

Table 4.14. EDS analysis of the specimen produced from powders of +63 μm

Location	Composition in wt%				
	Al	Si	V	Fe	Mg
silicide(1)	71.53	8.34	3.7	16.44	-
matrix (2)	80.24	13.88	1.03	4.85	-
Second phase free zone	86.15	4.33	1.96	7.57	-

In figure 4.27, Backscattered SEM micrograph of powder +63 micron is presented. Dispersoids up to 1-2 microns can be seen from figure. There is not significant difference in dispersoid size when it is compared with 4.26.
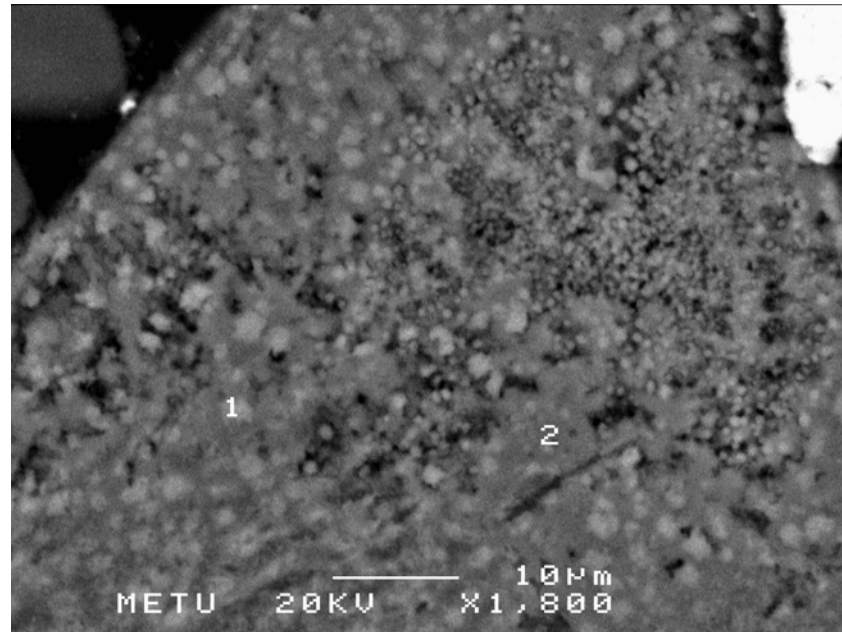

Figure 4.27 Backscattered SEM micrograph of +63 micron powder

Table 4.10. EDS analysis of +63 µm powder

Location	Composition in wt%				
	Al	Si	V	Fe	Mg
matrix(1)	75.21	7.95	2.83	13.75	0.26
matrix (2)	83.87	6.11	1.82	8.02	0.17

Figure 4.28 shows the Backscattered SEM Micrograph of specimen produced with +90 micron alloy powder b single action pressing before swagging. There are phases with angular shape which may be detrimental to the mechanical properties of the specimens. In a study of Kalkanlı et. al(27) , it was concluded that powders coarser than +63 microns contained angular and acicular shaped silicides.
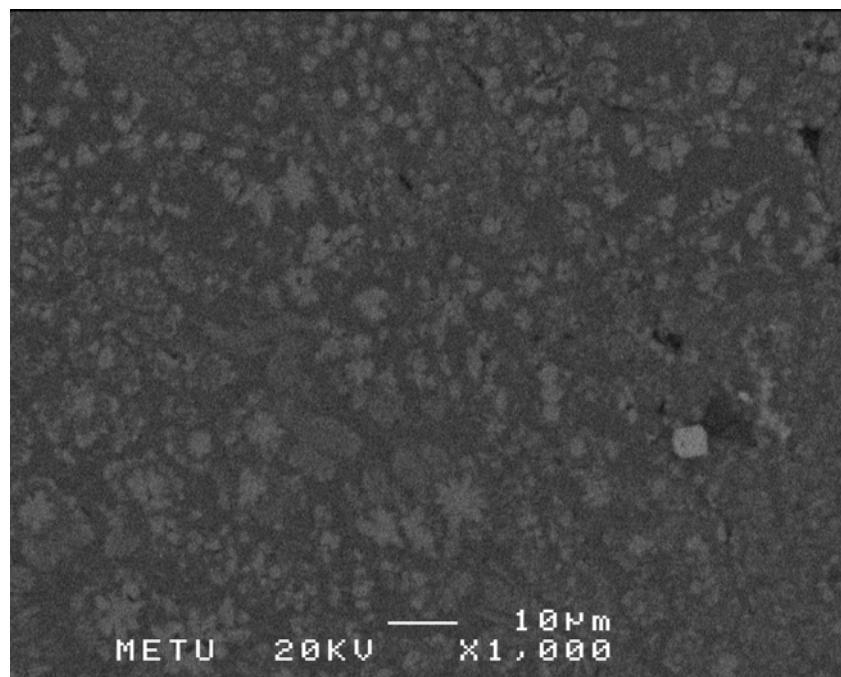

Fig. 4.28 Backscattered SEM Micrograph of specimen produced with powder size of +90 micron

In figure 4.29, Backscattered SEM micrograph of specimen produced with +63 micron by double pressing before swaging is presented. Some silicide rich regions can be seen as in the case of figure 4.26.
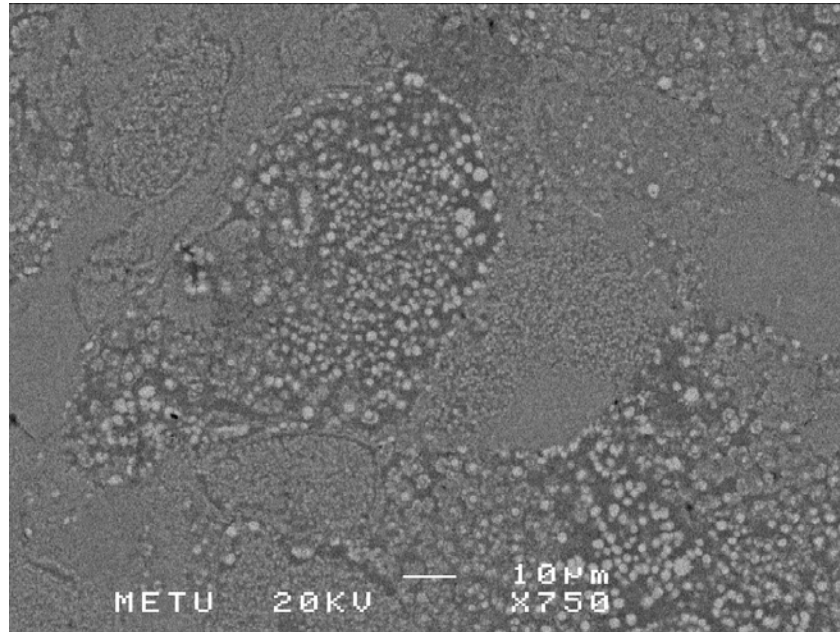

Fig. 4.29 Backscattered SEM micrograph of specimen produced with +63 micron by double pressing before swaging.

Backscattered SEM micrographs of 10% reinforced specimen produced from +63 micron alloy powder by double pressing before swaging is presented in figure 4.30, 4.31 .White big spots were TiC particles. In figure 4.31, a cluster of TiC was observed.

Fig. 4.30 Backscattered SEM micrograph of 10% TiC reinforced specimen produced from +63 micron alloy powder by double pressing before swaging. (vertical to the swaging direction)
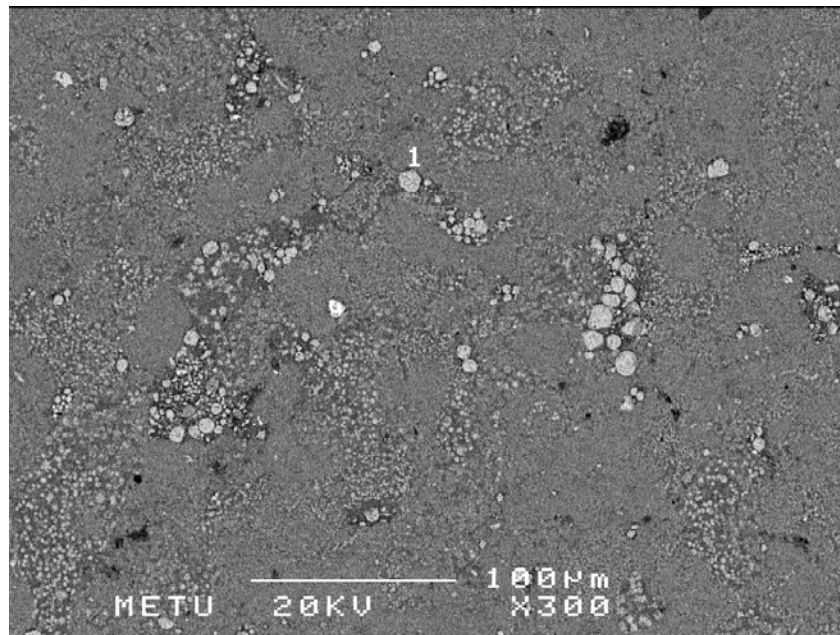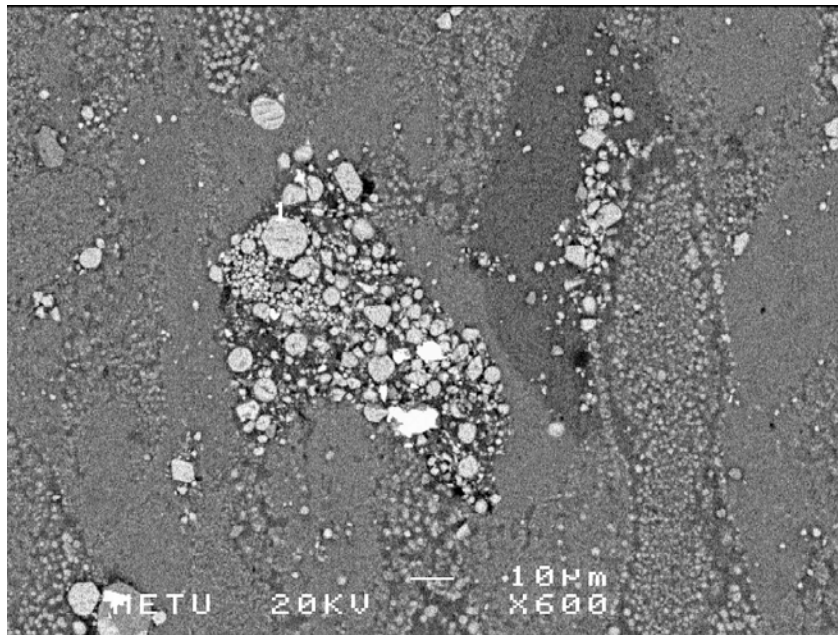
Fig. 4.31Backscattered SEM micrograph of 10% TiC reinforced specimen produced from +63 micron alloy powder by double pressing before swaging.

In figures 4.32 and 4.33 fractographs of 10% TiC reinforced specimens produced from +63 micron alloy powder by double pressing and by using canned loose powder before swaging are presented, respectively.

Figure 4.32 Fractograph of 10% TiC reinforced specimens produced from +63 micron alloy powder by double pressing
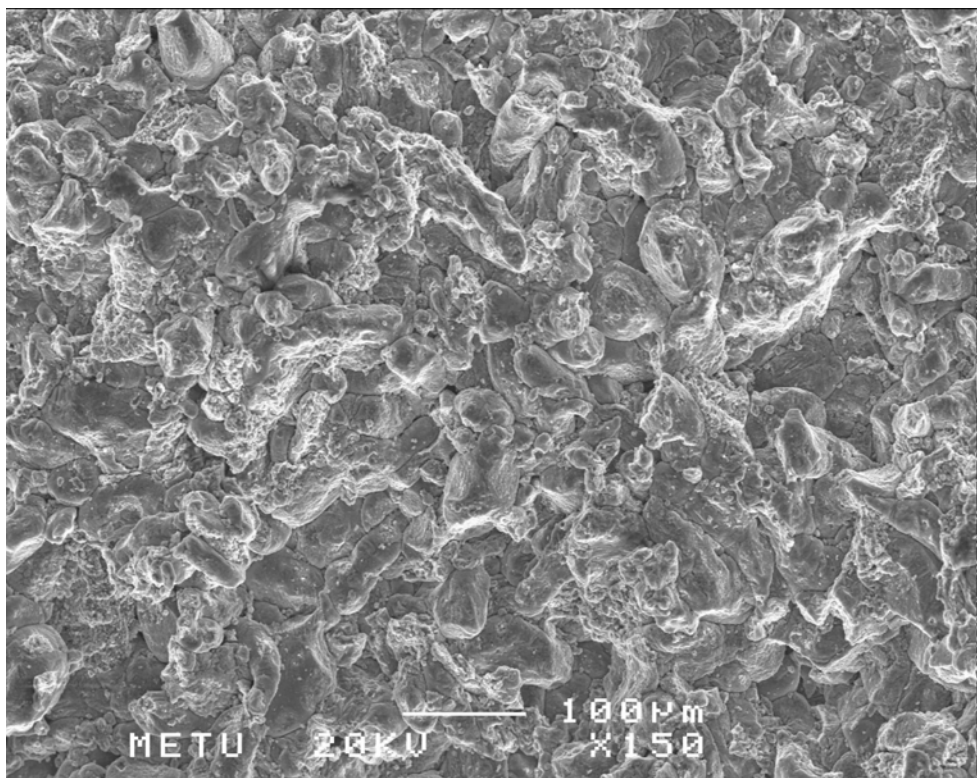
Figure 4.33 Fractograph of 10% TiC reinforced specimens produced from +63 micron alloy powder by using canned loose powder

In figure 4.34, SEM micrograph of 10% TiC reinforced specimens produced from +63 micron alloy powder by using canned loose powder is presented. TiC particles and dispersoids can be observed from the figure. TiC particle size varies between 1to 7 microns and they formed agglomarates.
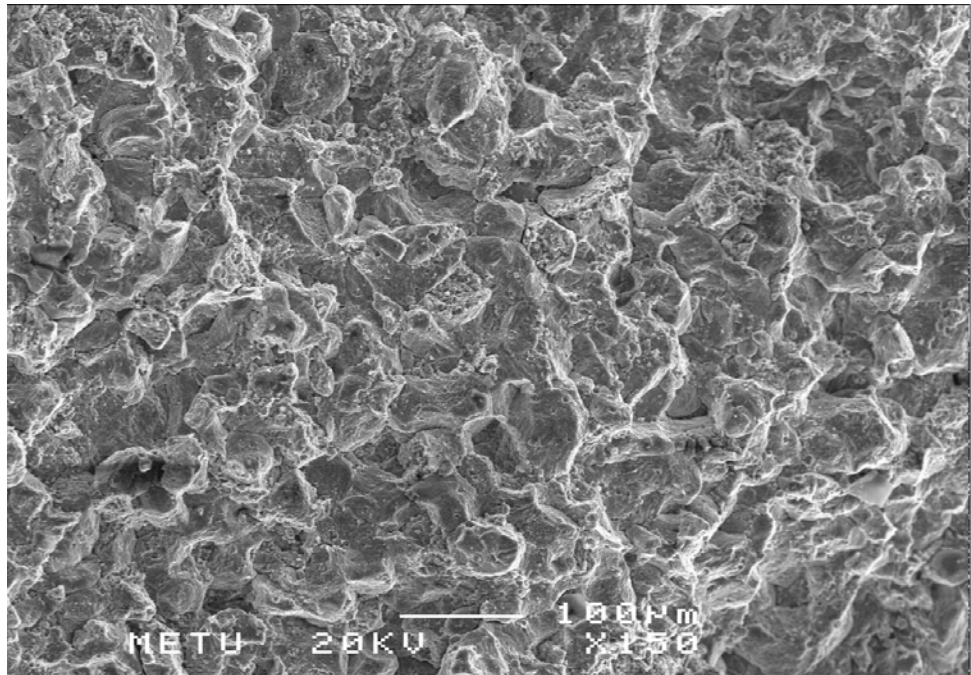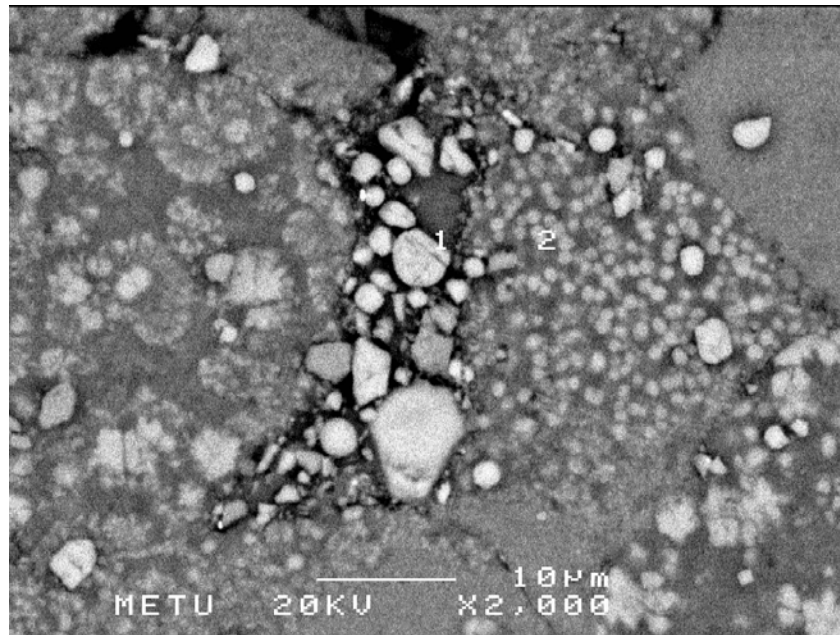

Figure 4.34 SEM micrograph of 10% TiC reinforced specimens produced from +63 micron alloy powder by using canned loose powder

4.7 Metallographic Study

Figures 4.35-4.38   show the optical micrographs of the alloy powders in different sizes. From these figures it can be stated that most of the powders for different sizes had rounded and ligament shape.
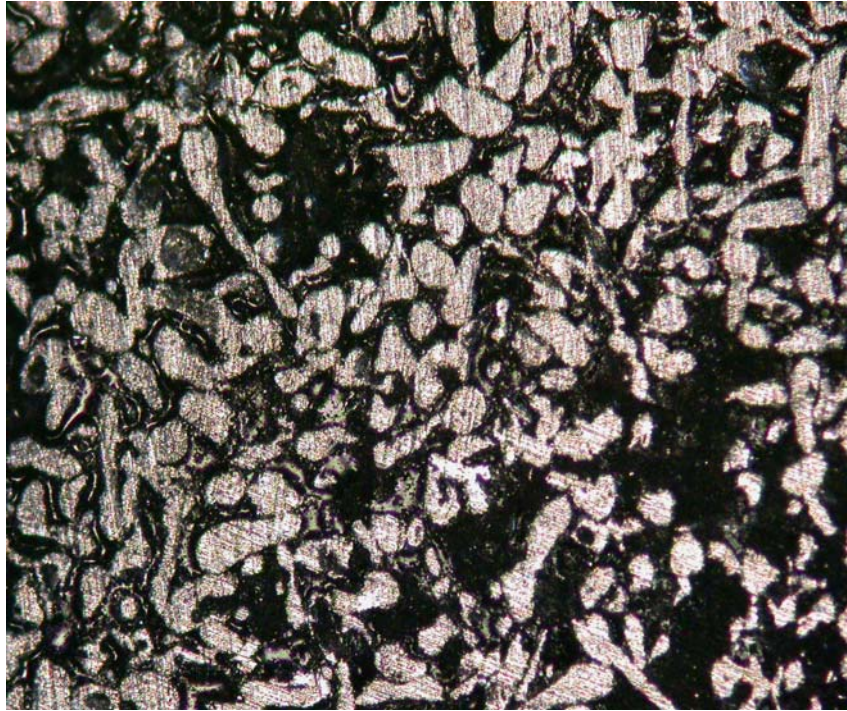
Figure 4.35 Optical micrograph of the alloy powder of +90µm (X50)
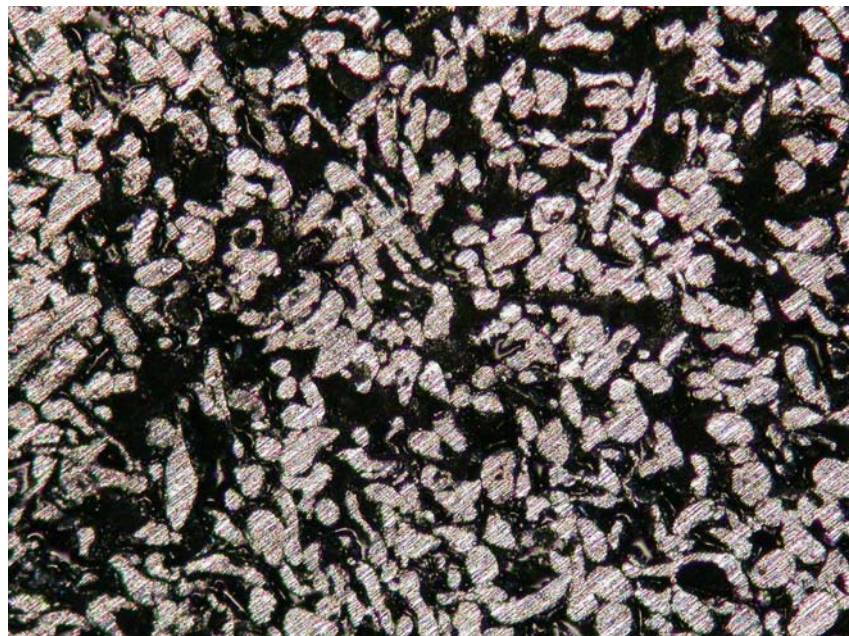
Figure 4.36 Optical micrograph of the alloy powder of +63µm (X50)

Figure 4.37 Optical micrograph of the alloy powder of +53μm (X50)
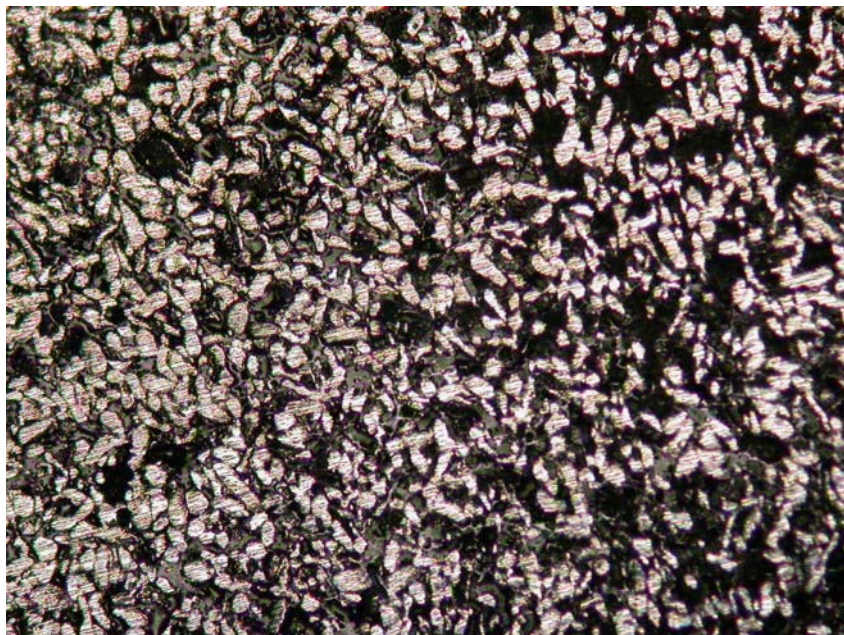
Figure 4.38 Optical micrograph of the alloy powder of +45μm (X50)

CHAPTER 5

CONCLUSIONS

In this study; experimental procedure was carried out in order to produce three point bending specimens from air atomized AlFeVSi alloy powders by hot dynamic consolidation method. Conclusion remarks can be stated as;

(i)   The alloy powders were in rounded and ligament shape.

(ii) There was no problem of layered structure which deteriorate mechanical properties as in the case of extrusion of alloy powders.

(iii) Porosity measurement of the three point bending specimens showed that the specimen density were very close to the theoretical density for specimens that were produced by single and double action pressing. High porosity of the specimens produced from powders smaller than 38μm may be attributed to the high interparticle friction due to the small initial powder size.

(iv) Hardness values of the specimens were inversely proportional to the powder size. The hardness values increases with decreasing powder size. Also hardness values of specimens varied by the processing conditions. The hardness values obtained for specimens produced by double action pressing before swaging were higher than the hardness values of specimens produced by using canned loose powder and single action pressing.

(v)   The cross like precipitates formed only near the outer surface of the specimens produced with +53 μm size powders by single action pressing were possibly $Al_{0.7}Fe_3Si_{0.3}$ phase.

(vi) Spherical silicides existing in the alloy powders had retained their shape after processing.

(vii) DSC results show that melting point of the alloy is around 575°C and no significant phase transformation peak was detected on the curves confirming the microstructural stability up to the melting temperature.

(viii) Flexural strength of some specimens could not be measured due to the delamination cracks which were vertical to the swaging direction.

(ix) The surface cracks can be formed due to the high density gradients caused by single action pressing and high H/D ratio. Surface cracks were also observed at specimens which were produced by double action pressing but although lower compaction pressures were applied higher maximum flexural stresses were obtained in these specimens. There was not any delamination crack in the specimens of canned loose powder but flexural strength of these specimens were lower than the ones produced by double action pressing due to higher uniform porosity compared to double and single pressed ones.

(x) The three point bending test of metal matrix composite specimens produced by 10% TiC addition showed that maximum flexural stress values increased in a significant amount while 20% TiC addition did not result in such an increase.

CHAPTER 6

SUGGESTIONS FOR FUTURE WORK

There may be changes in the processing method to obtain higher strength materials. Specimens were hot swaged only two times because of the the dimensions of three point bending tests. By changing the mechanical test (e.g. compression test), further swaging can be applied. Also, since the alloy is generally used at elevated temperatures, hot tensile testing and elastic modulus determination can be performed.

REFERENCES

1. Y.B. Liu, S.C. Lim, L. Lu, M.O. Lai , Journal of Materials Science, 29, 1994, 1999-2007

2. I.A.İbrahim, F.A. Mohammed, E.J. Lavernia, Journal of Materials Science, 26,1991,1137-1156

3. M.J Tan, X. Zhang, Materials Science and Engineering, A244, 1998, 80-85

4. .J.M. Torralbaa, C.E. da Costab, F. Velasco, Journal of Materials Processing Technology, 133, 2003, 203-206

5. V.R.V. Ramanan, D.J. Skinner and M.S. Zedalis, Materials Science and Engineering A, 134, 1991, 912-916,

6. S.J.Harris, AGARD Lectures Senes no. 174, New Light Alloys,1990, 21-24

7. Kenneth G. Kreider, Metallic Matrix Composites, Vol 4, 1974

8. S.Suresh A.Mortensen A.Needleman, Fundamentals of Metal Matrix Composites,   1993

9. Y.Wu, E.J.Lavernia, Scripta Metallurgica et Materalia, 27, 1992, 173-178

10. G.O.Donnal, L. Looney, Materials Science and Engineering A, 303, 2001, 292-301

11. X.Xia, H.J.Mcqueen, H.Zhu, Applied Composite Materials, 9, 2002, 17-31

12. X.C.Tong, A.K. Ghosh, Journal of Materials Science, 36, 2001, 4059-4069

13. Advances in metal matrix composites M.A.Taha N.A.El-Mahallawy

14. Powder Metallurgy Science, Randall M.German

15. Wolfgang G.J.Bunk, Materials Science and Enginnering A, 134, 1991, 1087-1097

16. W.J.Park, S.Ahn, Nack J. Kim, Materials Science and Engineering A, 189, 1994, 291-299

17. Ruangdaj Tangstri, Richard Dashwood, Henry Mcshane, Science Asia, 30, 2004, 33-41

18. S.K.Das, R.L.Bye, Materials Science and Engineering A, 134, 1991, 1103-1106

19. D.J.Skinner, R.L. Bye, D. Raynould and A.M. Brown, Scripta Metallurgica, 20, 1986, 867-872

20. S. Mitra, Scripta Matallurgica, Vol 27, 1992, p521-526,

21. R.E.Franck and J.A.Hawk, Scripta Metallurgica, Vol 23, 1989, p113-118,

22. Ruangdaj Tongsri, Jane Minay, Richard Thackray, Richard Dashwood, Henry Mcshaneb, Science Asia, 30, 2004

23. A.K. Srivastava, S.N.Ojha S.Ranganathan, Metallurgical and Materials Transactions A, 29A, 1998, 2205-2219

24. Ruangdaj Tongsri, Richard Dashwood and Henry Mcshaneb, Science Asia, 30, 33-412004

25. W.J.Park, S.Ahn, Nack J.Kim, Materials Science and Engineering A, 189, 1994, 291-299

26. Jian-Quiang Wang, Mei Kuang Tseng, Xiu-Fang Chen, Bao-Jin Zhang and Ze Xianyu, Materials Science and Engineering A, 1994, 179/A180, 412-415,

27. A. Kalkanli and E.E. Oren, Powder Metallurgy, Vol 46, 2003, 324-328

28. S.Mitra, T.R.McNelley, Metallurgical Transactions A, 24A, 1993, 2589-2592

29. Sunghak Lee, D.Y.Lee and Nack J.Kim, Materials Science and Engineering A, 1991, 33-44

30. R. Hambleton, H. Jones, W.M. Rainforth, Materials Science and Engineering A, 304–306, 2001, 524–528

31. V.Radmilovic, G.Thomas, Materials science and Engineering, A132, 1991, 171-179

32. Brian Ralph, H.C. Yuen, W.B. Lee, Journal of Materials Processing Technology,

33. Powder Metallurgy for Engineers, R.H.T. Dixon and A.Clayton

34. Casting and Forming Processes in Manufacturing, E.P.Degarmo, J.T. Black,P.H. Kohser

APPENDIX

51-1193

Wavelength= 1.79028

α−Al13(Fe.V)3Si

Aluminum Iron Silicon Vanadium

d(A)	Int	h	k	l
4.37	37	2	2	0
3.97	19	3	1	0
3.66	13	2	2	2
2.77	48	4	2	1
2.55	40	4	2	2
2.47	15	5	1	0
2.21	51	4	4	1
2.16	59	5	3	0
2.10	27	6	0	0
2.08	100	6	1	0
2.04	78	6	1	1
1.96	37	5	4	0
1.86	20	6	3	1
1.27	19	9	4	1

Rad.:   λ: Filter: d−sp:

Cut off: Int.:   I/Icor.:

Ref: Wang, J et al., Int. J. Non−Equilibrium Proc., 10, 83 (1997)

Sys.: Cubic   S.G.: P

a: 12.60   b: c: A: C:

α: β: γ: Z: 8   mp:

Ref: Ibid.

Dx: 3.615   Dm: SS/FOM: F_{14} = (0.162 , 83)

The elements were melt−spun into ribbons, then quenched. Al92.8 Ce0.28 Fe4.3 La0.15 Nd0.05 Pr0.02 Si1.7 V0.7. PSC: cP136. Mwt: 544.33. Volume[CD]: 2000.38.

51-1193

α-Al13(Fe.V)3Si

Aluminum Iron Silicon Vanadium

Rad.:	λ:	Filter:		d-sp.
Cut off:	Int.:		I/Icor.:	

Ref: Wang. J et al., Int. J. Non-Equilibrium Proc., 10, 83 (1997)

Sys.: Cubic			S.G.: P		
a: 12.60	b:	c:	A:		C:
α:	β:	γ:	Z: 8	mp:	

Ref: Ibid.

Dx: 3.615   Dm: SS/FOM: F14 = (0.162 , 83)

Wavelength= 1.79026

2θ	Int	h	k	l
23.640	37	2	2	0
26.061	19	3	1	0
28.313	13	2	2	2
37.707	48	4	2	1
41.101	40	4	2	2
42.495	15	5	1	0
47.787	51	4	4	1
48.965	59	5	3	0
50.460	27	6	0	0
50.980	100	6	1	0
52.053	78	6	1	1
54.349	37	5	4	0
57.535	20	6	3	1
89.631	19	9	4	1

The elements were melt-spun into ribbons, then quenched. Al92.8 Ce0.28 Fe4.3 La0.15 Nd0.05 Pr0.02 Si1.7 V0.7. PSC: cP136. Mwt: 544.33. Volume[CD]: 2000.38.

89-3657

Al

Aluminum

Aluminum

Rad.: CuKa1   λ: 1.54060   Filter: d-sp: Calculated
Cut off: 17.7   Int.: Calculated   I/Icor.:   4.10
Ref: Calculated from ICSD using POWD-12++
Ref: Straumanis, M.E., J. Appl. Phys., 30, 1965 (1959)

Sys.: Cubic			S.G.: Fm3̄m (225)		
a: 4.04954	b:	c:	A:		C:
α:	β:	γ:	Z: 4	mp:	

Ref: Ibid.

Dx: 2.699   Dm: 2.698   ICSD # : 044321

Wavelength= 1.79026

d(A)	Int	h	k	l
2.338	999 *	1	1	1
2.0247	456	2	0	0
1.4317	232	2	2	0
1.2209	229	3	1	1
1.169	62	2	2	2

Peak height intensity. PSC: cF4. No R value given. At least one TF missing. Mwt: 26.98. Volume[CD]: 66.41.

89-3657

Al

Aluminum

Aluminum

2 θ	Int	h	k	l
45.022	999 *	1	1	1
52.475	456	2	0	0
77.395	232	2	2	0
94.298	229	3	1	1
99.943	62	2	2	2

Rad.: CuKa1   λ: 1.54060   Filter: d-sp: Calculated

Cut off: 17.7   Int.: Calculated   I/Icor.:   4.10
Ref: Calculated from ICSD using POWD-12++
Ref: Straumanis, M.E., J. Appl. Phys., 30, 1965 (1959)

Sys.: Cubic   S.G.: Fm$\bar{3}$m (225)

a: 4.04954   b: c: A: C:

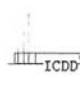α: β: γ: Z: 4   mp:

Ref: Ibid.

Dx: 2.699   Dm: 2.698   ICSD # : 044321

Peak height intensity. PSC: cF4. No R value given. At least one
TF missing. Mwt: 26.98. Volume[CD]: 66.41.

45-1204

Al0.7Fe3Si0.3

Aluminum Iron Silicon

d(A)	Int	h	k	l
3.32	7	1	1	1
2.875	3	2	0	0
2.033	100	2	2	0
1.7338	2	3	1	1
1.659	1	2	2	2
1.437	12	4	0	0
1.319	1	3	3	1
1.285	1	4	2	0
1.173	19	4	2	2
1.016	6	4	4	0
.9092	8	6	2	0
.830	2	4	4	4

Rad.: CuKa1   λ: 1.540598   Filter: d-sp: Calculated

Cut off: Int.: Calculated   I/Icor.:

Ref: Hubbard, C., Oak Ridge National Laboratory, High Temp.
Mat. Lab., Oak Ridge, TN, USA, Private Communication, (1993)

Sys.: Cubic   S.G.: Fm$\bar{3}$m (225)

a: 5.7502   b: c: A: C:

α: β: γ: Z: 4   mp:

Ref: Cowdery, S., Kayser, F., Mater. Res. Bull., 14, 91 (1979)

Dx: 6.807   Dm: SS/FOM: F_{12} = 316(.0022 , 17)

The lattice parameter for Al0.9 Fe3 Si0.1: a=5.7792; Al0.8 Fe Si0.2:
a=5.7647; Al0.6 Fe Si0.4: a=5.7357. Bi F3 type. PSC: cF16. Mwt:
194.85. Volume[CD]: 190.13.

45-1204　　　　　　　　　　　　　　　　　　　　　　　　　　　Wavelength= 1.79026

Al0.7Fe3Si0.3

Aluminum Iron Silicon

2θ	Int	h	k	l
31.283	7	1	1	1
36.281	3	2	0	0
52.246	100	2	2	0
62.166	2	3	1	1
65.268	1	2	2	2
77.027	12	4	0	0
85.459	1	3	3	1
88.240	1	4	2	0
99.386	19	4	2	2
123.430	6	4	4	0
159.814	8	6	2	0
	2	4	4	4

Rad.: CuKa1　λ: 1.540598　Filter:　　　　　d-sp: Calculated

Cut off:　　　Int.: Calculated　　　I/Icor.:

Ref: Hubbard, C., Oak Ridge National Laboratory, High Temp.
Mat. Lab., Oak Ridge, TN, USA, Private Communication, (1993)

Sys.: Cubic　　　　　　　　S.G.: Fm3m (225)

a: 5.7502　b:　　c:　　A:　　　C:

α:　　β:　　γ:　　Z: 4　mp:

Ref: Cowdery, S., Kayser, F., Mater. Res. Bull., 14, 91 (1979)

Dx: 6.807　　Dm:　　　SS/FOM: F_{12} = 316(.0022 , 17)

The lattice parameter for Al0.9 Fe3 Si0.1: a=5.7792; Al0.8 Fe Si0.2:
a=5.7647; Al0.6 Fe Si0.4: a=5.7357. Bi F3 type. PSC: cF16. Mwt:
194.85. Volume[CD]: 190.13.